Since January 2020 Elsevier has created a COVID-19 resource centre with free information in English and Mandarin on the novel coronavirus COVID-19. The COVID-19 resource centre is hosted on Elsevier Connect, the company's public news and information website.

European Journal of Operational Research xxx (xxxx) xxx

Contents lists available at ScienceDirect

European Journal of Operational Research

journal homepage: www.elsevier.com/locate/ejor

Design of control strategies to help prevent the spread of COVID-19 pandemic

Seyyed-Mahdi Hosseini-Motlagh*, Mohammad Reza Ghatreh Samani, Shamim Homaei

School of Industrial Engineering, Iran University of Science and Technology, University Ave, Narmak, Tehran 16846, Iran

ARTICLE INFO

Article history:
Received 17 November 2020
Accepted 9 November 2021
Available online xxx

Keywords:
Or in developing countries
COVID-19
Resource allocation
Transmission rate
Multi-stage stochastic programming
Fuzzy uncertainty model

ABSTRACT

This paper proposes control strategies to allocate COVID-19 patients to screening facilities, health facilities, and quarantine facilities for minimizing the spread of the virus by these patients. To calculate the transmission rate, we propose a function that accounts for contact rate, duration of the contact, age structure of the population, susceptibility to infection, and the number of transmission events per contact. Moreover, the COVID-19 cases are divided into different groups according to the severity of their disease and are allocated to appropriate health facilities that provide care tailored to their needs. The multi-stage fuzzy stochastic programming approach is applied to cope with uncertainty, in which the probability associated with nodes of the scenario tree is treated as fuzzy variables. To handle the probabilistic model, we use a more flexible measure, *Me* measure, which allows decision-makers to adopt varying attitudes by assigning the optimistic-pessimistic parameter. This measure does not force decision-makers to hold extreme views and obtain the interval solution that provides further information in the fuzzy environment. We apply the proposed model to the case of Tehran, Iran. The results of this study indicate that assigning patients to appropriate medical centers improves the performance of the healthcare system. The result analysis highlights the impact of the demographic differences on virus transmission, and the older population has a greater influence on virus transmission than other age groups. Besides, the results indicate that behavioral changes in the population and their vaccination play a key role in curbing COVID-19 transmission.

1. Introduction

"May God bless us and help us to defeat COVID-19 all together."

In the last decades, a rising number of outbreaks have occurred globally due to climate changes, demographic changes, and habitat destruction (Nkengasong, 2020). Ebola virus outbreak (2013), Middle East respiratory syndrome (MERS) coronavirus outbreak (2012), H1N1 flu outbreak (2009), and severe acute respiratory syndrome (SARS) outbreak (2002) are examples of epidemic outbreaks during the last two decades. Such situations disrupt people's lives and impose heavy social and economic burdens on affected communities (Silal, 2021). Recently, a novel coronavirus, SARS-CoV-2, has caused a new outbreak which quickly changed into a pandemic and has infected a significant number of people around the world (Nikolopoulos et al. 2021). Therefore, due to the rising number of outbreaks and their impacts on societies, effective responses should be prepared to cope with such outbreaks and mitigate their effects.

This new coronavirus is different from MERS-CoV (coronavirus caused MERS) and SARS-CoV (coronavirus causes SARS). It has a higher transmission rate and easily spreads between humans. As of 6 June 2021, there has been reported 176,066,274 COVID-19 (C-19) confirmed cases and 3801,301 total deaths (Worldometers, 2021). Notably, the death rate due to C-19 is lower than the other known coronavirus diseases; however, due to high transmissibility, the death toll of C-19 has exceeded the death toll of MERS and SARS (WHO, 2020a). This virus is transmitted mainly through the droplets (generated from talking, coughing, and sneezing) when a susceptible person is in close contact with an infected person. The population's age structure also affects the transmission of the disease (Zhang et al., 2020). If the C-19 spread is not appropriately contained, a considerable number of people will be infected by this virus; accordingly, the healthcare system will be overwhelmed by patients and will face a capacity shortage. High economic costs will also be imposed on the communities (Nagurney, 2021). Therefore,

* Corresponding author.
E-mail address: motlagh@iust.ac.ir (S.-M. Hosseini-Motlagh).

https://doi.org/10.1016/j.ejor.2021.11.016
0377-2217/

decision-makers (DMs) need to take effective strategies to control the outbreak and slow and stop the C-19 transmission.

The infected patients' age and their medical conditions affect the risk and severity of the C-19 disease; accordingly, the C-19 virus can cause mild symptoms such as caught and fever to severe symptoms such as shortness of breath and kidney failure. The risk of severe disease is also higher for older adults and those with underlying conditions such as diabetes and cancers (Liu et al., 2020a, 2020b). Based on the disease severity, the treatment process of the patients and their required care equipment will be different. Patients with severe illness may need advanced care in intensive care units (ICUs), oxygen therapy, or ventilation. However, mild cases may not need inpatient care, and they can be isolated in community facilities such as stadiums and hotels (WHO, 2020b). The limited resources and limited capacities of health facilities (HFs) are critical factors during outbreaks (Li et al., 2021). Therefore, regarding the community spread of C-19, the limited capacity of HFs, and the scarcity of advanced care resources, the patients with different illness severity should be assigned to the appropriate facilities that provide medical services tailored to their needs. In this case, patients can receive their required care effectively, and the resources will be fairly assigned to patients; thus, C-19 cases can access life-saving treatment without compromising public health objectives. Moreover, after improving the conditions of the C-19 patients, they will be transferred to quarantine facilities (QFs) during their recovery process.

Regarding the novelty of the C-19 virus and the enormous amount of uncertainty surrounding the healthcare system, information on this disease is not yet fully known. Uncertainties can compromise the reliability of the decisions and deteriorate the performance of the healthcare system. During the COVID-19 outbreak (CVO), the demand for health services is highly uncertain, and handling this uncertainty will provide optimal allocation decisions. According to the above, DMs should adopt reliable strategies to cope with uncertainties during outbreaks.

Several aspects of different outbreaks have been discussed in the following review papers. Chowell and Nishiura (2014) reviewed the developed mathematical models for containing the Ebola virus outbreak in West Africa and explored the impacts of different interventions on spreading the virus. Dimitrov and Meyers (2014) investigated the different mathematical models for forecasting the spread pattern of infectious diseases. Dasaklis et al. (2012) studied the role of logistics operations in containing epidemic outbreaks.

Several techniques can be used to control, manage, and contain disease outbreaks in affected areas. We categorized the relevant literature into two main streams: forecasting disease spread during outbreaks, and allocating and distributing emergency resources during outbreaks. In the first stream, the researchers used mathematical models and simulation methodologies to estimate the progression of the disease during the outbreak and analyzed the impact of control interventions on the spread of the disease. Das et al. (2008) proposed a simulation model to mimic the spread of influenza, in which several features such as demographic, psychological, and epidemiological features were considered in the model. Pandey et al. (2014) presented a stochastic model to estimate the transmission of the Ebola virus before and after adopting control measures such as curfew and social distance. In this model, different sources of infection such as community, HF, and funeral were taken into account. Hackl and Dubernet (2019) used an agent-based approach to simulate the spread of seasonal influenza disease in urban areas by considering the interaction between individuals and their behaviors during a day.

In the second stream, researchers aimed to efficiently allocate limited emergency resources among affected people regarding the dynamics of the outbreaks. Tanner and Ntaimo (2010) developed a fuzzy stochastic programming approach to determine the optimal allocation of vaccines and vaccination policies during an epidemic outbreak under uncertainty in contact rate and vaccine efficacy. Koyuncu and Erol (2010) used a mathematical model to find the optimal resource allocation during the influenza pandemic to minimize the virus transmission and the outbreak's duration. Rachaniotis et al. (2012) developed a deterministic model to determine the optimal allocation of limited resources during the influenza pandemic in a mass vaccination setting. The concept of job deterioration was incorporated into the problem. He and Liu (2015) developed a model to manage the distribution of medical services during infectious disease outbreaks. The psychological and physical effects of the outbreak on the affected people were considered in the model. Anparasan and Lejeune (2018) provided a mathematical model to support the response supply chain during cholera outbreaks in developing countries.

In some papers, the problem of disease spread and resource allocations were investigated simultaneously. Tebbens and Thompson (2009) presented a model to manage the spread of multiple infectious diseases. The limited budget was allocated to eradicate the diseases, and policies adopted to control the spread of the diseases were prioritized due to the budget constraints. Ren et al. (2013) provided a model to control the propagation of the smallpox disease. They aimed to determine the optimal allocation of vaccines regarding the limited resources and the optimal control measures concerning transmission intensity in the infected areas. Yarmand et al. (2014) developed a mathematical model to estimate the spread of seasonal influenza. They proposed a two-phase model to distribute the vaccines to infected people. In this study, vaccines are distributed among people considering the uncertainty in outbreak dynamics in the first phase. Then, the vaccines are redistributed in the second phase based on the outcomes of the first phase. Ekici et al. (2014) investigated the propagation of influenza disease, designed a network to allocate resources among infected people, and determined the optimal working hours of distribution centers in each period.

Wanying et al. (2016) provided a response plan for anthrax attacks, in which they assessed the number of infected people and distributed antibiotics among HFs based on the patients' disease severity in those HFs. Liu and Zhang (2016) forecasted the uncertain demand for medical resources during an influenza outbreak using a transmission model and assigned the medical resources to HFs based on the predicted demands. They also updated their estimated demands based on the collected data from HFs. Dasaklis et al. (2017) provided a transmission model to estimate the progression of the disease during a smallpox attack. Then, they proposed a deterministic model to manage the supply of emergency resources considering healthcare and transportation capacities. Büyüktahtakın et al. (2018) provided a mathematical model for controlling the spread of the Ebola disease and determining the optimal amount of resources in health centers. Liu et al. (2020a, 2020b) provided an epidemic-logistic model to determine the dynamic of H1N1 influenza, allocate the resources, and determine the number of required isolation wards.

Uncertainty plays a key role in decision-making processes during outbreaks; however, a few of the reviewed papers, such as Ekici et al. (2014), Yarmand et al. (2014), and Tanner and Ntaimo (2010), considered uncertainty in their presented problems. Ekici et al. (2014) incorporated demand uncertainty in their proposed model and used a dynamic approach to handle it. Yarmand et al. (2014) considered uncertainty in vaccination outcome, which is dealt with a two-stage stochastic approach. Tanner and Ntaimo (2010) considered uncertainty in disease parameters and used a fuzzy stochastic approach to cope with it.

Recently, some researchers have investigated the CVO to provide efficient strategies for controlling this outbreak. In the fields of the supply chains, Ivanov (2020) investigated the effect of dis-

ruptions originated from the CVO on the performance of the supply chains using simulation methodology under several scenarios such as local and epidemic spread of the virus. Peirlinck et al. (2020) presented a model to estimate the spread of the C-19 virus before adopting control measures in the affected areas. Govindan et al. (2020) proposed a decision support system for managing the demand for medical care during CVO. This system categorizes patients into several groups based on their ages and medical conditions, prioritizes them in terms of their conditions, and connects them to appropriate service providers. Mehrotra et al. (2020) proposed a two-stage stochastic model for managing the allocation of ventilators during CVO. In this model, different demand scenarios are considered, and the idle ventilators can be shared between HFs based on the risk levels. Weissman et al. (2020) proposed a deterministic model for forecasting the spread of the C-19 disease. The model is used to obtain the optimal decision for allocating emergency resources and managing hospital capacities effectively. Lin et al. (2020) proposed a model to predict the transmission of the C-19 virus and investigated the effect of preventive measures and people's behavior on spreading the diseases.

Manufacturing and distributing vaccines are key challenges during CVO (Alam et al., 2021; Sinha et al., 2021). Georgiadis and Georgiadis (2021) developed a mathematical model for planning the C-19 vaccine supply chain while minimizing its cost. A rolling horizon algorithm is used to handle the uncertainties in the daily plan of vaccination centers. Abbasi et al. (2020) proposed a model to determine optimal allocation decisions in an integrated vaccine supply chain. The model aims to minimize the risk of infection, and transshipping vaccines between the centers is allowed. An age-based model was presented by Chen et al. (2020) to determine the optimal policy for vaccine allocation that resulted in a minimized number of infected cases and deaths.

In short, in the reviewed literature, some researchers investigated the performance of the supply chains during health crises from different aspects; however, the effects of uncertainties on supply chains are still to be adequately investigated. Considering uncertainty in such situations will result in more reliable decisions. Moreover, the research on the healthcare supply chain during the CVO is at a nascent stage, and the resource allocation problems during this uncertain environment need further investigations. Assigning patients to the centers providing appropriate medical care is also a key factor in allocating emergency resources, which is not appropriately addressed in CVO. This factor prevents the misuse of limited resources, and consequently, optimal care will be provided for patients on time. In addition to properly allocating resources during CVO, policymakers aim to prevent the further spread of the disease. Therefore, reliable estimation of the spread of the C-19 by considering the transmission characteristic of the virus and adopting effective strategies influences the mitigation of the outbreak significantly.

In this paper, we propose a mathematical model to allocate the C-19 cases to health centers so that the spread of the C-19 virus by these patients is minimized. The transmission rate of C-19 depends on the rate of contact between an infected and a susceptible case, the probability of disease transmission, the proportion of infected cases, and the population's age structure. Besides, C-19 cases are categorized into three groups regarding the severity of their illness and their background of the disease; consequently, different types of HFs, including isolation facilities (HF_1s), general hospitals (HF_2s), and specialized hospitals (HF_3s), are considered, and patients are assigned to HFs that provide medical services tailored to their needs. The number of suspected C-19 cases is considered uncertain in order to reflect real-world conditions properly. The uncertainty in this parameter affects allocation decisions, transmission rate, and reliability of the model. To cope with the uncertainty, a multi-stage fuzzy stochastic programming (MFSP) approach is applied to the model. In this approach, the decisions can be updated as more information is realized over time; as a result, the performance of the healthcare system improves. Besides, the probability of the nodes of the scenario tree is considered as fuzzy parameters. Finally, *Me* measure is used to handle the fuzzy objective function and chance constraints. By applying this measure, the lower and upper bounds of the optimal decision are provided; consequently, more information is provided for DMs, and they can adopt their attitude to their decisions. The main contributions of this study are as follows:

- Proposing a function for estimating the C-19 transmission rate based on the rate of contacts between infected and susceptible cases, the probability of the C-19 transmission per contact, and the susceptibility of any age group to C-19 infection.
- Proposing a mathematical model for minimizing the C-19 transmission rate and determining the optimal assignment of C-19 cases to health centers by considering their limited capacities.
- Developing the MFSP approach to deal with uncertainty and applying *Me* measure to handle fuzzy objective function and chance constraints.
- Applying the proposed model to a real case to address the practicality of the model.
- This paper answers the following main questions:
- How to slow the spread of C-19 disease?
- How to assign the patients to health centers in order to manage the limited capacity efficiently during CVO?
- How to cope with uncertainties to make reliable decisions during CVO?

The structure of the paper is as follows. The problem is described in Section 2, and the mathematical formulation is explained in Section 3. The proposed MFSP approach is presented in Section 4. The case study is addressed in Section 5, and the results and sensitivity analyses are provided in Section 6. Finally, the conclusion, managerial insights, and future avenues are presented in Section 7.

2. The formal description of the transmission-allocation problem

This paper presents an emergency supply chain problem to allocate C-19 patients to the health centers in an efficient manner while the disease transmission minimizes. The schematic view of the proposed network is shown in Fig. 1. First, the suspected C-19 cases of each region refer to C-19 SFs to be tested. After receiving the test results, a proportion of referred cases is released due to negative test results. The confirmed cases are assigned to HFs regarding the illness severity and background of the disease. We categorize the patients into three types: mildly ill patients (PT_1s), severely ill patients (PT_2s), and patients with underlying conditions (PT_3s). PT_1s have stable conditions, and they do not need inpatient settings; therefore, they are assigned to HF_1 in which mild cases are isolated to prevent the further spread of the virus.

The unstable patients, PT_2s and PT_3s, need inpatient care (such as oxygen therapy and ventilation), and therefore, they are transferred to hospitals. PT_2s are patients with severe disease, and they are allocated to HF_2s, while PT_3s (whether with severe or mild symptoms) are transferred to HF_3s to be treated according to their special medical conditions. Notably, during CVO, a proportion of the capacity of hospitals (HF_2s and HF_3s) is dedicated to C-19 patients, while routine services are provided for non-COVID-19 (non-C-19) patients simultaneously. The HFs are capacitated, and therefore, if the HF_3s are overwhelmed with PT_3s, this type of patient will be allocated to HF_2s (in case of having available capacity). Besides, the conditions of some of the mild cases who are isolated in HF_1s may deteriorate; such patients should be transferred to HF_2s.

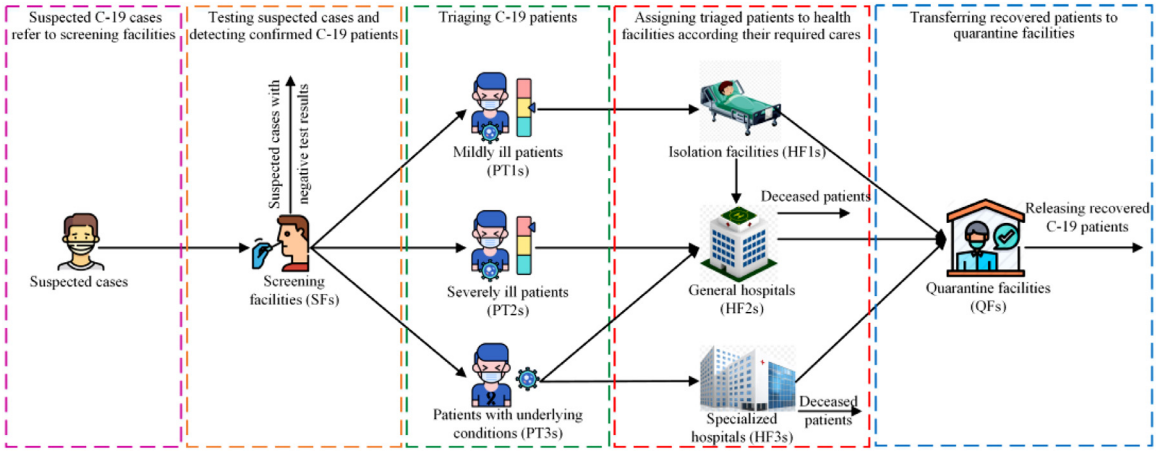

Fig. 1. The schematic view of the proposed network.

Furthermore, some of the patients will lose their lives due to the high severity of the illness. After patients recover from disease in each type of HF, they are transferred to QFs for monitoring their conditions. Also, this can prevent the spread of the virus since C-19 patients may be contagious after they have recovered. Finally, they are discharged from QFs. The proposed model aims to minimize the C-19 transmission and determine the optimal allocation of C-19 patients to health centers. We discuss below how to formulate the objective function of the proposed model.

2.1. The transmission rate of the C-19 virus

Each infected case that moves between two nodes (regions, SFs, HF_1s, HF_2s, HF_3s, and QFs) can transmit the C-19 to the susceptible cases. The rate of C-19 transmission (η) from C-19 patients to susceptible people depends on three factors: 1) the rate of contacts between an infected case with susceptible cases of age group g when the infected case travels from node n to node n' ($\mathbb{C}_{nn'g}$); 2) the probability of C-19 transmission during a contact between a C-19 case and a susceptible case of age group g; 3) the proportion of infected cases. Thus, we calculate η as follows (see Del Valle et al., 2013; Keeling & Eames, 2005):

$$\eta_{nn'gt} = \begin{pmatrix} rate\ of\ contact\ between\ an\ infected\ case\ and\ susceptible\ cases\ of\ age\ group\ g\ in\ the\ route\ connecting\ node\ n\ to\ node\ n' \end{pmatrix} \times \begin{pmatrix} probability\ of\ disease\ transmission\ to\ a\ susceptible\ case\ of\ age\ group\ g\ per\ contact \end{pmatrix} \begin{pmatrix} proportion\ of\ infected\ cases\ in\ the\ route\ connecting\ node\ n\ to\ node\ n' \end{pmatrix} = (\mathbb{C}_{nn'g}) \quad (\mathbb{S}_g \cdot \mathbb{P}_g) \quad \left(\frac{\mathbb{I}_{nn't}}{\mathbb{D}_{nn'}.\mathbb{M}_{nn'}}\right) \tag{1}$$

in which a mechanistically based function is used to obtain the contact rate as follows (see Heesterbeek & Metz, 1993; Roberts, 1996):

$$\mathbb{C}_{nn'g} = \frac{2.\mathbb{T}_g.\mathbb{D}_{nn'g}}{1 + 2.\mathbb{T}_g.\mathbb{D}_{nn'g} + \sqrt{1 + 4.\mathbb{T}_g.\mathbb{D}_{nn'g}}} \tag{2}$$

In this formulation, the contact rate ($\mathbb{C}$) is functions of the average duration of contact between a person of age group g and other persons ($\mathbb{T}_g$), and the density of the population of age g in the route (n,n') ($\mathbb{D}_{nn'g}$). The population density of regions is known, and the population density of a route depends on the population density of the regions that the route passes and the portion of the route placed in each region. In other words, the population density of the route (n,n') is calculated as follows:

$$\mathbb{D}_{nn'g} = \frac{\sum_{e=1}^{E} \mathbb{D}_{eg}.M_{enn'}}{\mathbb{M}_{nn'}} \forall n \neq n' \tag{3}$$

in which $\mathbb{D}_{eg}$ is the density of population of age g in region e and $M_{enn'}$ is a portion of the route (n,n'), which is placed in region e. Besides, $\mathbb{M}_{nn'}$ is the distance of route (n,n').

The susceptibility to C-19 infection varies by age, and therefore, we consider an age-varying susceptibility to the disease. The investigations show that children have a lower vulnerability to the C-19 rather than adults, and older adults are the most vulnerable group to the virus (Davies et al., 2020). Therefore, we categorize the susceptible population into three age groups, children with 0 to 14 years old, adults with 15 to 64 years old, and older adults with more than 64 years old. The susceptibility to C-19 infection for people of age group g is shown by $\mathbb{S}_g$. Furthermore, the probability of disease transmission to a susceptible individual of age g ($\mathbb{P}_g$) is an exponential function of the average duration of contact between an individual of age g and other persons ($\mathbb{T}_g$) and the average number of transmission events per contact ($\mathbb{N}$), as shown below (see Del Valle et al., 2013).

$$\mathbb{P}_g = 1 - e^{-\mathbb{N}.\mathbb{T}_g} \tag{4}$$

Regarding the above descriptions, the probability of C-19 transmission in each contact equals $\mathbb{S}_g.\mathbb{P}_g$.

Finally, the transmission rate depends on the proportion of the infected cases in each route (n,n'), which is calculated as the ratio of the number of infected cases transfers between nodes n and n' in each period ($\mathbb{I}_{nn't}$) and the number of people in this route. We estimate the number of the people in route (n,n') by multiplying the density of the population in the area that route (n,n') passes ($\mathbb{D}_{nn'}$) and the distance of the route (n,n') ($\mathbb{M}_{nn'}$). In this study, the number of infected cases transferred from node n to node n' is variable, and it is determined by solving the model. For simplification, we rewrite Formulation (1) as follows:

$$\eta_{nn'gt} = \left(\mathbb{C}_{nn'g}\right).\left(\mathbb{S}_g.\mathbb{P}_g\right).\left(\frac{\mathbb{I}_{nn't}}{\mathbb{D}_{nn'}.\mathbb{M}_{nn'}}\right) = \left(\mathbb{C}_{nn'g}\right).\left(\mathbb{S}_g.\mathbb{P}_g\right).\left(\frac{1}{\mathbb{D}_{nn'}.\mathbb{M}_{nn'}}\right).\mathbb{I}_{nn't} = \eta'_{nn'g}.\mathbb{I}_{nn't} \forall n \neq n' \tag{5}$$

in which $\eta'_{nn'g}$ is a parameter, and $\mathbb{I}_{nn't}$ is a decision variable obtained by solving the presented model in Section 3. The number of susceptible cases of age group g infected by having contact with

a C-19 patient is calculated by $\eta_{nn'gt} = \eta'_{nn'g}.\mathbb{I}_{nn't}$, and the number of infected persons of any age group by an infected case equals $\sum_{g=1}^{G} \eta_{nn'gt} = \mathbb{I}_{nn't} \sum_{g=1}^{G} \eta'_{nn'g} = \mathbb{I}_{nn't}.\eta'_{nn'}$.

Covid-19 is a novel virus, and there is little information about that. It is evident that C-19 patients can transmit the virus to susceptible people before their treatment (when they are transferring from regions to SFs (η^{RS}), from SFs to hospitals (η^{SH}), and between hospitals (η^{HH})). However, some researchers declared that the C-19 patients could be contagious after their treatment; therefore, we consider that the C-19 transmission occurs after patients are discharged from the hospital; therefore, we consider that the patients are transferred to QFs (η^{HQ}) after discharging from hospitals to avoid further C-19 transmission. In this study, we also consider that the facilities are capacitated. Therefore, the facilities may reject some patients due to the lack of capacity. However, these cases are infected patients, and they transmit the virus to other people. Thus, we consider the transmission rate for such patients in each region as follows:

$$\eta^{R}_{egt} = \begin{pmatrix} rate\ of\ contact\ between\ an \\ infected\ case\ and\ susceptible \\ cases\ of\ age\ group\ g\ in\ region\ e \end{pmatrix} \times \begin{pmatrix} probability\ of\ disease \\ transmission\ to\ a \\ susceptible\ case\ of\ age \\ group\ g\ per\ contact \end{pmatrix} \begin{pmatrix} proportion\ of \\ infected\ cases \\ in\ region\ e \end{pmatrix} = (\mathbb{C}^{R}_{eg})(\mathbb{S}_g.\mathbb{P}_g)\left(\frac{\mathbb{I}_{et}}{\mathbb{R}_e}\right) \quad (6)$$

In this formulation, η^{R}_{egt} shows the number of infected cases by a C-19 patient whom facilities reject due to lack of capacity. η^{R}_{egt} is a function of three factors: 1) the rate of contacts between an infected case and susceptible cases of age group g in region e ($\mathbb{C}^{R}_{eg}$); 2) the probability of C-19 transmission during a contact between a C-19 patient and a susceptible individual of age group g; 3) the proportion of infected cases. $\mathbb{C}^{R}_{eg}$ is calculated as follows:

$$\mathbb{C}^{R}_{eg} = \frac{2.\mathbb{T}_g.\mathbb{D}_{eg}}{1 + 2.\mathbb{T}_g.\mathbb{D}_{eg} + \sqrt{1 + 4.\mathbb{T}_g.\mathbb{D}_{eg}}} \quad (7)$$

in which the contact rate depends on the average contact time ($\mathbb{T}_g$) and the population density of region e. $\mathbb{S}_g$ and $\mathbb{P}_g$ are obtained based on the descriptions mentioned above. Finally, the proportion of the infected cases in region e in each period is calculated as the ratio of the number of infected cases in region e at each period ($\mathbb{I}_{et}$) to the number of population in region e ($\mathbb{R}_e$). $\mathbb{I}_{et}$ is a decision variable, and it is determined by solving the model. In order to simplify, we convert the Formulation (6) into the following formulation:

$$\eta^{R}_{egt} = \left(\mathbb{C}^{R}_{eg}\right).(\mathbb{S}_g.\mathbb{P}_g).\left(\frac{\mathbb{I}_{et}}{\mathbb{R}_e}\right) = \left(\mathbb{C}^{R}_{eg}\right).(\mathbb{S}_g.\mathbb{P}_g).\left(\frac{1}{\mathbb{R}_e}\right).\mathbb{I}_{et} = \eta'^{R}_{egt}.\mathbb{I}_{et} \quad (8)$$

The total number of infected cases by a C-19 patient in region e in period t equals $\sum_{g=1}^{G} \eta^{R}_{egt} = \mathbb{I}_{et} \sum_{g=1}^{G} \eta'^{R}_{egt} = \mathbb{I}_{et}.\eta''^{R}_{et}$.

According to the descriptions mentioned above, the model's objective function seeks to minimize the virus transmission from infected cases to susceptible individuals in the presented network during the planning horizon. It involves transmitting the virus from C-19 patients when transferred from regions to SFs, from SFs to HFs, between HFs, from HFs to QFs, and the virus transmission from patients rejected from different facilities to susceptible people. The following assumptions are considered in this study:

- Suspected cases are classified into several groups according to the regions they are located in, and each group is assumed to be located at the center of each region due to its uniform population distribution.
- The test result is prepared on the same day the test is taken
- SFs, HF_1s, HF_2s, HF_3s, and QFs are capacitated, and the assigned patients will be rejected by the facilities in case of facing a capacity shortage in these facilities.
- There are no patients in the facilities at the beginning of the planning horizon.

The main decisions of the presented model are as follows:

- The optimal location of SFs, HFs, and QFs.
- The number of suspected C-19 cases allocated to SFs.
- The number of C-19 cases allocated to HFs and QFs.
- The number of PT_3s who are assigned to HF_2s due to limited capacities.
- The optimal capacity of HFs assigned to C-19 patients.

3. Modeling framework

In this section, the proposed mathematical formulation is presented.

Appendix A. Notations

The following notations are used in the proposed model in Section 3.1.

Sets	
E	Set of regions, $e = \{1, 2, \ldots, E\}$
I, I''	Set of candidate locations for SFs, $i = \{1, 2, \ldots, I\}$
J, J', J''	Set of types of patients, $j = \{1, 2, 3\} = \{PT_1, PT_2, PT_3\}$
K, K', K''	Set of types of HFs, $k = \{1, 2, 3\} = \{HF_1, HF_2, HF_3\}$
L, L', L''	Set of candidate locations of HFs, $l = \{1, 2, \ldots, L\}$
Q	Set of candidate locations of QFs, $q = \{1, 2, \ldots, Q\}$
T	Set of time periods, $t = \{1, 2, \ldots, T\}$
Parameters	
α_{et}	The number of suspected cases in region e in period t
β_{it}	The percentage of suspected cases in SF i whose tests results are negative in period t
γ_{ijt}	The percentage of suspected cases in SF i whose tests results are positive and are categorized in patient type j in period t
δ_{klt}	The percentage of deceased C-19 cases in HF l of type k in period t
ε^{H}_{klt}	The percentage of C-19 cases released from HF l of type k in period t
ε^{Q}_{qt}	The percentage of C-19 cases released from QF q in period t
$\sigma_{klk'l't}$	The percentage of patients transferred from HF l of type k to HF l' of type k' in period t
ζ_{kl}	The average number of non-C-19 cases admitted to HF l of type k
ρ^{S}_{i}	The capacity of SF i
ρ^{H}_{kl}	The capacity of HF l of type k
ρ^{Q}_{q}	The capacity of QF q
λ^{S}_{i}	The cost of opening SF i
λ^{H}_{kl}	The cost of opening HF l of type k
λ^{Q}_{q}	The cost of opening QF q
μ^{S}_{i}	The operating cost in SF i
μ^{H}_{jkl}	The operating cost of hospitalizing a patient of type j in HF l of type k
μ^{Q}_{q}	The operating cost in QF q
θ^{RS}_{ei}	The cost of transporting a patient from region e to SF i
θ^{SH}_{ikl}	The cost of transporting a patient from SF i to HF l of type k
$\theta^{HH}_{klk'l'}$	The cost of transporting a patient from HF l of type k to HF l' of type k'
θ^{HQ}_{klq}	The cost of transporting a patient from HF l of type k to QF q
ξ	The penalty cost of rejecting a patient by facilities (SFs, HFs, QFs)
υ	The penalty cost of allocating a patient to an HF that does not provide medical services according to his/her need
ω^{S}_{ei}	equals 1 if SF i is located in region e
ω^{H}_{ekl}	equals 1 if HF l of type k is located in region e
Ψ	The total budget
M	A large number

Decision variables

U_i^S	equals 1 if an SF is established in candidate location i; otherwise, 0
U_{kl}^H	equals 1 if an HF of type k is established in candidate location l; otherwise, 0
U_q^Q	equals 1 if a QF is established in candidate location q; otherwise, 0
X_{eit}	The number of suspected cases in region e assigned to SF i in period t
Y_{ijklt}	The number of C-19 cases of type j transferred from SF i to HF l of type k in period t
Z_{klqt}	The number of recovered patients transferred from HF l of type k to QF q in period t
P_{eit}^S	The number of suspected C-19 cases in region e who are rejected by SF i in period t
P_{ijklt}^H	The number of C-19 patients of type j in SF i who are rejected by HF l of type k in period t
P_{klqt}^Q	The number of recovered patients of type k who are hospitalized in HF l and are rejected by QF q in period t
C_{kl}	The percentage of capacity of HF l of type k assigned to C-19 patients
EC	The establishment cost
OC	The operating cost
TC	The transportation cost
PC	The penalty cost

Auxiliary variables

V_{klt}^H	The number of available patients in HF l of type k in period t
V_{qt}^Q	The number of available patients in QF q in period t

Auxiliary binary variable

B_{it}^S, B_{klt}^H, B_{qt}^Q

Objective decision variable

TT	The transmission rate of the C-19 virus

Appendix B. Results

The number of assigned cases to different facilities is shown in the following table.

3.1. The mathematical formulation

In this section, the mathematical formulation of the proposed location-allocation problem is presented. The objective function aims to minimize the spread of the C-19 virus as follows:

$$\begin{aligned}\min TT = &\sum_{e=1}^{E}\sum_{i=1}^{I}\sum_{t=1}^{T}\eta_{ei}^{''RS}.X_{eit}.\sum_{j=1}^{3}\gamma_{ijt} + \sum_{i=1}^{I}\sum_{j=1}^{3}\sum_{k=1}^{3}\sum_{l=1}^{L}\sum_{t=1}^{T}\eta_{ikl}^{''SH}.Y_{ijklt}\\ &+\sum_{l=1}^{L}\sum_{l'=1}^{L}\sum_{t=1}^{T}\eta_{ll'}^{''HH}.\sigma_{1l2l't}.V_{1lt}^H + \sum_{k=1}^{3}\sum_{l=1}^{L}\sum_{q=1}^{Q}\sum_{t=1}^{T}\eta_{klq}^{''HQ}.Z_{klqt}\\ &+\sum_{e=1}^{E}\eta_e^{''R}.\Bigg(\sum_{i=1}^{I}\sum_{t=1}^{T}P_{eit}^S.(1-\beta_{it})\\ &+\sum_{i=1}^{I}\sum_{j=1}^{3}\sum_{k=1}^{3}\sum_{l=1}^{L}\sum_{t=1}^{T}P_{ijklt}^H.\omega_{ei}^S\\ &+\sum_{k=1}^{3}\sum_{l=1}^{L}\sum_{q=1}^{Q}\sum_{t=1}^{T}P_{klqt}^Q.\omega_{ekl}^H\Bigg)\end{aligned} \tag{9}$$

In fact, this objective function aims to minimize the C-19 transmission rate in each route and each region regarding Formulations (5) and (8). The number of infected cases who go to SF i from region e equals the proportion of suspected cases whose test results are positive ($\gamma_{ijt}.X_{eit}$). The number of infected cases transferred from SF i to HF l of type k is Y_{ijklt}. The number of infected cases transferred from HF_1 to HF_2 equals the proportion of PT_1 whose conditions deteriorate ($\sigma_{1l2l't}.V_{1lt}^H$). Finally, the number of recovered patients transferred from HF l of type k to QF q is Z_{klqt}. Besides, the rejected patients by different facilities (SFs, HFs, and QFs) can spread the C-19 in the regions, which is considered in the last term of Formulation (9). subject to

$$EC = \sum_{i=1}^{I}\lambda_i^S.U_i^S + \sum_{k=1}^{3}\sum_{l=1}^{L}\lambda_{kl}^H.U_{kl}^H + \sum_{q=1}^{Q}\lambda_q^Q.U_q^Q \tag{10}$$

Table B1
The number of C-19 suspected cases assigned to SFs and the number of occupied beds by C-19 patients in HFs and QFs during the planning horizon under each scenario.

SF	scenario	1	2	3	4	5	6	7	8	9	10	11	12	13	14
	LAM	858	1031	1204	1030	1203	1376	1202	1375	1548	1032	1205	1378	1203	1376
	UAM	1034	1242	1450	1241	1449	1657	1448	1656	1864	1243	1450	1660	1450	1658
	scenario	15	16	17	18	19	20	21	22	23	24	25	26	27	
	LAM	1376	1375	1549	1722	1206	1379	1552	1378	1551	1723	1550	1723	1896	
	UAM	1658	1657	1865	2074	1452	1661	1869	1659	1867	2076	1866	2074	2283	
HF_1	scenario	1	2	3	4	5	6	7	8	9	10	11	12	13	14
	LAM	182	203	223	202	224	244	223	243	264	204	225	245	224	244
	UAM	220	244	269	244	269	293	268	293	318	246	271	296	270	295
	scenario	15	16	17	18	19	20	21	22	23	24	25	26	27	
	LAM	245	245	265	286	226	247	267	246	267	288	267	287	308	
	UAM	295	293	320	344	273	297	322	297	322	346	321	346	371	
HF_2	scenario	1	2	3	4	5	6	7	8	9	10	11	12	13	14
	LAM	40	45	51	47	52	57	53	58	64	47	52	57	53	58
	UAM	49	55	61	56	63	69	64	70	77	56	63	69	64	70
	scenario	15	16	17	18	19	20	21	22	23	24	25	26	27	
	LAM	58	60	65	70	53	58	63	60	65	70	66	71	76	
	UAM	70	72	78	84	64	70	77	72	78	84	80	86	92	
HF_3	scenario	1	2	3	4	5	6	7	8	9	10	11	12	13	14
	LAM	33	38	43	39	44	50	46	51	56	47	44	50	46	51
	UAM	37	44	50	47	54	60	51	57	63	56	54	60	55	61
	scenario	15	16	17	18	19	20	21	22	23	24	25	26	27	
	LAM	51	52	57	62	46	51	56	52	57	62	58	63	69	
	UAM	61	63	69	75	55	61	67	63	69	75	70	76	83	
QF	scenario	1	2	3	4	5	6	7	8	9	10	11	12	13	14
	LAM	40	56	71	59	75	90	79	94	109	46	62	77	65	81
	UAM	43	58	80	68	86	105	87	105	124	49	63	80	66	85
	scenario	15	16	17	18	19	20	21	22	23	24	25	26	27	
	LAM	94	85	100	116	52	68	83	72	87	103	91	106	122	
	UAM	105	89	108	126	63	82	100	86	105	124	109	128	147	

$$OC = \sum_{e=1}^{E}\sum_{i=1}^{I}\sum_{t=1}^{T}\mu_i^S.X_{eit} + \sum_{j=1}^{3}\sum_{k=1}^{3}\sum_{l=1}^{L}\sum_{t=1}^{T}\mu_{jkl}^H.V_{klt}^H + \sum_{q=1}^{Q}\sum_{t=1}^{T}\mu_q^Q.V_{qt}^Q \tag{11}$$

$$\begin{aligned} TC = &\sum_{e=1}^{E}\sum_{i=1}^{I}\sum_{t=1}^{T}\theta_{ei}^{RS}.X_{eit} + \sum_{i=1}^{I}\sum_{j=1}^{3}\sum_{k=1}^{3}\sum_{l=1}^{L}\sum_{t=1}^{T}\theta_{ikl}^{SH}.Y_{ijklt} \\ &+ \sum_{k=1}^{3}\sum_{l=1}^{L}\sum_{q=1}^{Q}\sum_{t=1}^{T}\theta_{klq}^{HQ}.Z_{klqt} \\ &+ \sum_{l=1}^{L}\sum_{l'=1}^{L}\sum_{t=1}^{T}\theta_{1l2l'}^{HH}.\sigma_{1l2l't}.V_{k=1,lt}^H \end{aligned} \tag{12}$$

$$\begin{aligned} PC = \xi.&\left(\sum_{e=1}^{E}\sum_{i=1}^{I}\sum_{t=1}^{T}P_{eit}^S + \sum_{i=1}^{I}\sum_{j=1}^{3}\sum_{k=1}^{3}\sum_{l=1}^{L}\sum_{t=1}^{T}P_{ijklt}^H + \sum_{k=1}^{3}\sum_{l=1}^{L}\sum_{q=1}^{Q}\sum_{t=1}^{T}P_{klqt}^Q\right) \\ &+ \nu.\sum_{i=1}^{I}\sum_{l=1}^{L}\sum_{t=1}^{T}Y_{i,j=2,k=3,lt} \end{aligned} \tag{13}$$

$$EC + OC + TC + PC \le \Psi \tag{14}$$

Constraints (10)–(13) calculate total establishment cost, total operating cost, total transportation cost, and total penalty cost, respectively. The presented model aims to find the optimal number and location of SFs, HFs, and QFs. The facilities can be established in the obtained optimal locations, and the opening costs are considered for these facilities (Constraint (10)). The suspected cases refer to SFs, and they are tested for C-19 disease there. Thus, we consider operating costs for suspected cases in these facilities. An operating cost is also considered for assigned patients to different types of HFs and QFs (Constraint (11)). Furthermore, the transportation cost is considered for transferring suspected cases from regions to SFs, transferring C-19 patients from SFs to HFs, transferring patients between HFs, and transferring patients from HFs to QFs (Constraint (12)). Finally, some patients are rejected by facilities due to the lack of capacities, and a penalty cost is assigned to these patients. In some cases, PT_3s are assigned to HF_2s due to the lack of capacity in HF_3s, which are not compatible with these patients' needs; therefore, we consider penalty costs for such cases (Constraint (13)). Constraint (14) represents the budget constraint.

$$\sum_{i=1}^{I}(X_{eit} + P_{eit}^S) \ge \alpha_{et}, \qquad \forall e, t \tag{15}$$

$$\rho_i^S.B_{it}^S \le \sum_{e=1}^{E}X_{eit} \le \rho_i^S.U_i^S, \qquad \forall i, t \tag{16}$$

$$\sum_{e=1}^{E}P_{eit}^S \le M.B_{it}^S, \qquad \forall\ i, t \tag{17}$$

In the presented network, the suspected cases in each region are assigned to opened SFs which are capacitated. In each region and each period, there are a number of suspected cases that will be assigned to SFs or will be rejected by SFs due to limitation of capacity in those facilities, which is shown in Constraint (15). The capacities of opened SFs are also limited, and therefore, the number of suspected cases refers to an SF should be less than its capacity, as shown in Constraint (16). As mentioned before, some suspected cases cannot refer to the assigned SFs due to lack of capacity, and Constraint (17) shows that opened SFs can reject the suspected cases. It is evident that suspected cases will be rejected by an opened SF when that SF is filled to capacity, guaranteed by Constraints (16) and (17). To do so, we defined a binary variable, B_{it}^S. This variable equals 0 if the SF i is not opened, and it guarantees that P_{eit}^S equals 0. On the other hand, if SF i is opened, B_{it}^S can be equal to 0 or 1. In fact, if SF i is filled ($B_{it}^S = 1$), suspected cases can be rejected by SF i; otherwise, $B_{it}^S = 0$, and consequently, no suspected cases are rejected by SF i due to sufficient capacity in that SF. In other words,

$$B_{it}^S = \begin{cases} 1 & \text{if SF } i \text{ is opened and is filled in period } t \\ 0 & \text{if SF } i \text{ is not opened or if SF } i \text{ is opened and is not filled in period } t \end{cases}$$

$$\sum_{l=1}^{L}(Y_{ijklt} + P_{ijklt}^H) \ge \gamma_{ijt}.\sum_{e=1}^{E}X_{eit}, \qquad \forall i, t;\ j = 1, k = 1 \tag{18}$$

$$\sum_{l=1}^{L}(Y_{ijklt} + P_{ijklt}^H) \ge \gamma_{ijt}.\sum_{e=1}^{E}X_{eit}, \qquad \forall i, t;\ j = 2, k = 2 \tag{19}$$

$$\begin{aligned} &\sum_{l=1}^{L}\left(Y_{ijklt} + P_{ijklt}^H\right) + \sum_{l'=1}^{L}(Y_{ijk'l't} + P_{ijk'l't}^H) \ge \gamma_{ijt}.\sum_{e=1}^{E}X_{eit}, \\ &\forall i, t;\ j = 3, k = 3, k' = 2 \end{aligned} \tag{20}$$

In the next step, the suspected cases referred to SFs will be tested, the number of patients of each type will be determined, and they will be assigned to different types of HFs based on their conditions. Also, some patients will be rejected by hospitals due to capacity limitations. The confirmed PT_1s in each SF will be assigned to HF_1s or rejected by these facilities, as Constraint (18) shows. Constraint (19) also states that PT_2s will be assigned to HF_2s or rejected by these facilities. PT_3s will be assigned to HF_3s or assigned to HF_2s in case of capacity limitation in HF_3s. Thus, Constraint (20) implies that the PT_3s will be assigned to HF_2s or HF_3s or rejected by these HFs.

$$\sum_{i=1}^{I}Y_{ijklt} = V_{klt}^H, \qquad \forall l;\ j = 1, k = 1, t = 1 \tag{21}$$

$$\begin{aligned} &V_{kl(t-1)}^H.\left(1 - \varepsilon_{kl(t-1)}^H - \sum_{l'=1}^{L}\sigma_{klk'l'(t-1)}.U_{k'l'}^H\right) + \sum_{i=1}^{I}Y_{ijklt} = V_{klt}^H, \\ &\forall l, t \ge 2;\ j = 1, k = 1, k' = 2 \end{aligned} \tag{22}$$

After confirmed cases are allocated to hospitals, it should be guaranteed that the number of allocated patients to each type of HF is less than its capacity. Constraint (21) indicates that the number of available PT_1s in an HF_1 in the first period equals the number of PT_1s transferred from SFs to this facility. It is assumed that there are no patients in these facilities at the beginning of the planning horizon. In the following periods, a proportion of the capacity has been filled by patients who were already in the hospitals and are still receiving treatments. Notably, the conditions of some PT_1s in HF_1s may deteriorate. In such cases, they will be transferred from HF_1s to HF_2s to receive their required care. Also, a proportion of patients will be discharged in each period ($T \ge 2$). Therefore, the number of available PT_1s in an HF_1 in each period ($T \ge 2$) equals the number of allocated PT_1s to this facility in this period addition to the number of patients in the previous period by considering the number of patients transferred to opened HF_2s due to deteriorating their conditions and the number of discharged patients, as shown in Constraint (22). Notably, the number of transferred and discharged patients is determined at the end of each period, and therefore, they affect the facility's capacity in the

next period.

$$\sum_{i=1}^{I}(Y_{ijklt}+Y_{ij'klt})=V^{H}_{klt},\qquad \forall l;\ j=2,k=2,j'=3,t=1 \tag{23}$$

$$V^{H}_{kl(t-1)}.\left(1-\varepsilon^{H}_{kl(t-1)}-\delta_{kl(t-1)}\right)+\sum_{i=1}^{I}(Y_{ijklt}+Y_{ij'klt})+\sum_{l''=1}^{L}\sigma_{k''l''kl(t-1)}.V^{H}_{k''l''(t-1)}=V^{H}_{klt},$$
$$\forall l,t\geq 2;\ j=2,k=2,j'=3,j''=1,k''=1 \tag{24}$$

As mentioned before, some PT_3s may be assigned to HF_2s due to a lack of capacity in HF_3s. Thus, the number of available patients in each HF_2 in the first period equals the number of transferred PT_2s and PT_3s to this facility, as Constraint (23) shows. In HF_2s, a proportion of available patients will be released or deceased in each period, the number of which is determined at the end of each period ($T\geq 2$). It is mentioned that some PT_1s are transferred to HF_2s, the number of which is determined at the end of each period. Therefore, the number of available patients in each HF_2 in each period ($T\geq 2$) equals the sum of the number of patients who have been in the HF_2 from the previous period (considering the number of discharged and deceased patients), the number of patients assigned to the HF_2 in that period, and the number of patients transferred from HF_1s to the HF_2 in the previous period, as shown in Constraint (24).

$$\sum_{i=1}^{I}Y_{ijklt}=V^{H}_{klt},\qquad \forall l;\ j=3,k=3,t=1 \tag{25}$$

$$V^{H}_{kl(t-1)}.\left(1-\varepsilon^{H}_{kl(t-1)}-\delta_{kl(t-1)}\right)+\sum_{i=1}^{I}Y_{ijklt}=V^{H}_{klt},$$
$$\forall l,t\geq 2;\ j=3,k=3 \tag{26}$$

In HF3, the number of available patients in the first period equals the number of PT3s assigned to that HF3, since there are no patients in HF_3 at the beginning of the planning horizon, and there are no deceased or released patients in the first period, as shown in Constraint (25). Constraint (26) indicates that the number of available patients in each period ($T\geq 2$) equals the sum of the number of available patients in HF3s in the previous period (regarding the number of deceased and released patients at the end of that period) and the number of transferred patients from SFs to this facility in that period.

$$\rho^{H}_{kl}.B^{H}_{klt}\leq V^{H}_{klt}\leq \rho^{H}_{kl}.U^{H}_{kl},\qquad \forall l,t;\ k=1 \tag{27}$$

$$\sum_{i=1}^{I}P^{H}_{ijklt}\leq M.B^{H}_{klt},\qquad \forall l,t;\ j=1,k=1 \tag{28}$$

$$\rho^{H}_{kl}.C_{kl}+\zeta_{kl}\leq \rho^{H}_{kl}.U^{H}_{kl},\qquad \forall l,k=2,3 \tag{29}$$

$$\rho^{H}_{kl}.C_{kl}.B^{H}_{klt}\leq V^{H}_{klt}\leq \rho^{H}_{kl}.C_{kl},\qquad \forall l,t,k=2,3 \tag{30}$$

$$\sum_{i=1}^{I}P^{H}_{ijklt}+\sum_{i=1}^{I}P^{H}_{ij'klt}\leq M.B^{H}_{klt},\qquad \forall l,t;\ j=2,j'=3,k=2 \tag{31}$$

$$\sum_{i=1}^{I}P^{H}_{ijklt}\leq M.B^{H}_{klt},\qquad \forall l,t;\ j=3,k=3 \tag{32}$$

The number of available patients in each established HF (including HF_1, HF_2, and HF_3) in each period should be less than the capacity of that facility. As mentioned before, patients can be rejected by an opened HF if the HF is filled. These conditions are satisfied by Constraints (27) and (28) for HF_1. To do so, we define a binary variable that

$$B^{H}_{klt}=\begin{cases}1 & \text{if HF } l \text{ of type } k \text{ is opened and is filled in period } t\\ 0 & \text{if HF } l \text{ of type } k \text{ is not opened or if HF } l \text{ of type } k \text{ is opened and is not filled in period } t\end{cases}$$

In HF_2 and HF_3, a proportion of the capacity is assigned to non-C-19 patients. Therefore, the number of C-19 and non-C-19 patients should be less than the capacity of opened HFs, as Constraint (29) shows. Constraint (30) guarantees that the number of available C-19 patients should be less than the allocated capacity to C-19 patients. Also, the C-19 patients will be rejected by HF_2 and HF_3 if the assigned capacity to C-19 patients is full, as Constraints (30–32) show.

$$\sum_{q=1}^{Q}(Z_{klqt}+P^{Q}_{klqt})\geq V^{H}_{klt}.\varepsilon^{H}_{klt},\qquad \forall k,l,t \tag{33}$$

$$\sum_{k=1}^{3}\sum_{l=1}^{L}Z_{klqt}=V^{Q}_{qt},\qquad \forall q;\ t=1 \tag{34}$$

$$V^{Q}_{q(t-1)}.\left(1-\varepsilon^{Q}_{q(t-1)}\right)+\sum_{k=1}^{3}\sum_{l=1}^{L}Z_{klqt}=V^{Q}_{qt},\qquad \forall q,t\geq 2 \tag{35}$$

$$\rho^{Q}_{q}.B^{Q}_{qt}\leq V^{Q}_{qt}\leq \rho^{Q}_{q}.U^{Q}_{q},\qquad \forall q,t \tag{36}$$

$$\sum_{k=1}^{3}\sum_{l=1}^{L}P^{Q}_{klqt}\leq M.B^{Q}_{qt},\qquad \forall q,t \tag{37}$$

The patients in each type of HFs, after their treatment, are discharged and assigned to QFs; however, they will be rejected by QFs in case of capacity shortage in these facilities, as shown in Constraint (33). The number of available recovered cases in each QF in the first period equals the number of assigned cases to that facility, as Constraint (34) shows. At the end of each period, some patients are in QFs, a proportion of whom will be released, and the remaining patients will fill a proportion of the facility capacity in the next period. Therefore, the number of available cases in a QF in each period ($T\geq 2$) equals the sum of the number of available cases in the QF since previous periods and the number of assigned cases to the QF in this period, as shown in Constraint (35). Constraint (36) indicates that the number of available cases in each opened QF should be less than its capacity. Also, the recovered cases can be rejected by opened QFs in case of capacity shortage. This condition is satisfied by Constraints (36) and (37). To do so, we define an auxiliary binary variable as follows:

$$B^{Q}_{qt}=\begin{cases}1 & if\ QF\ q\ is\ opened\ and\ is\ filled\ in\ period\ t\\ 0 & if\ QF\ q\ is\ not\ opened\ or\ if\ QF\ q\ is\ opened\ and\ is\ not\ filled\ in\ period\ t\end{cases}$$

$$U^{S}_{i},U^{H}_{kl},U^{Q}_{q},B^{S}_{it},B^{H}_{klt},B^{Q}_{qt}\in\{0,1\},\qquad \forall i,k,l,q,t \tag{38}$$

$$X_{eit},Y_{ijklt},Z_{klqt},P^{S}_{eit},P^{H}_{ijklt},P^{Q}_{klqt},C_{kl},V^{H}_{klt},V^{Q}_{qt}\geq 0,\qquad \forall e,i,j,k,l,q,t \tag{39}$$

Constraints (38) and (39) show the types of decision variables.

3.2. The linear counterpart of the proposed mathematical formulation

The proposed formulation is nonlinear due to the multiplication of a binary and a continuous variable in Constraints (22) and (30) ($V^H_{kl(t-1)}.U^H_{k'l'}$ and $C_{kl}.B^H_{klt}$). We convert the Constraints (22) into its linear form by defining a new positive variable ($F_{klk'l't}$) as follows (Psarris & Floudas, 1990):

$$V^H_{kl(t-1)}.\left(1-\varepsilon^H_{kl(t-1)}\right)-\sum_{l'=1}^{L}\sigma_{klk'l'(t-1)}.F_{klk'l'(t-1)}+\sum_{i=1}^{I}Y_{ijklt}=V^H_{klt},$$
$$\forall l, t\geq 2; j=1, k=1, k'=2 \quad (40)$$

$$F_{klk'l'(t-1)}\leq M.U^H_{k'l'}, \qquad \forall l, t\geq 2; k=1, k'=2 \quad (41)$$

$$F_{klk'l'(t-1)}\geq M.(U^H_{k'l'}-1)+V^H_{kl(t-1)}, \qquad \forall l, t\geq 2; k=1, k'=2 \quad (42)$$

$$F_{klk'l'(t-1)}\leq V^H_{kl(t-1)}, \qquad \forall l, t\geq 2; k=1, k'=2 \quad (43)$$

$$F_{klk'l't}\geq 0, \quad \forall l, t\geq 1; k=1, k'=2 \quad (44)$$

In these constraints, M is the upper value of $V^H_{kl(t-1)}$, which equals ρ^H_{kl}. The linear form of Constraint (30) is as follows (F'_{klt} is a positive variable):

$$\rho^H_{kl}.F'_{klt}\leq V^H_{klt}\leq \rho^H_{kl}.C_{kl}, \qquad \forall l, t; k=2,3 \quad (45)$$

$$F'_{klt}\leq M.B^H_{klt}, \qquad \forall l, t; k=2,3 \quad (46)$$

$$F'_{klt}\geq M.(B^H_{klt}-1)+C_{kl}, \qquad \forall l, t; k=2,3 \quad (47)$$

$$F'_{klt}\leq C_{kl}, \qquad \forall l, t; k=2,3 \quad (48)$$

$$F'_{klt}\geq 0, \qquad \forall l, t; k=2,3 \quad (49)$$

In the above constraints, M is the upper value of C_{kl} which equals 1.

4. Methodology

We live in a fast-changing world. We have limited knowledge about the future, and many uncertainties exist even if the past information is available. During the CVO, many factors (such as adopted policies and the public behavior toward the policies) affect healthcare systems; consequently, decisions should be made in a highly uncertain environment, and DMs should adopt suitable approaches to hedge against such uncertainties as much as possible. During this outbreak, an optimal allocation of resources is a critical factor that can significantly improve the performance of the healthcare system.

In the proposed location-allocation problem, the number of suspected cases in each period is highly dynamic. The number of diagnosed cases in SFs depends on this parameter. The amount of capacity filled by patients in HFs and QFs and the number of patients admitted to HFs and QFs is subject to this random parameter. Furthermore, this uncertain parameter arrives over time. In other words, this parameter is unknown now, but it will be realized in the future, and the realized information can update the decisions. Stochastic programming is applied to models in which some data is contaminated with random uncertainty. Notably, the decisions are made without prior knowledge of the entire data stream; however, such data is updated over time; consequently, the decisions are updated based on the revealed data. According to the above, we use stochastic programming to deal with uncertainty in the proposed network.

Two-stage stochastic programming (TSP) and multi-stage stochastic programming (MSP) are two of the most commonly used approach to hedge against uncertainties. In the TSP approach, some initial decisions (first-stage decisions) are made before the realization of the uncertain data, after which second-stage decisions are made regarding the realized data (Hosseini-Motlagh et al., 2020; Samani et al., 2020). In other words, it is assumed that the data arrives at one point in the planning horizon, and therefore, decisions can be updated at one point in time. However, the data can be realized in several points of the planning horizon. In such circumstances, MSP is an appropriate approach to cope with such uncertain parameters. In this approach, decisions can be revised as more data becomes available. Therefore, the decisions will be more reliable and flexible than the decisions made regarding the TSP approach. According to the above, we applied the MSP approach to the proposed model.

MSP approach is a more general form of the TSP. In the MSP, there are several stages, and decision variables are divided into several groups based on the related stages. In this approach, the main issue is what data is available to DMs at one stage when making relevant decisions to this stage. In fact, stages are the point of time in which new information is realized. In the MSP, the evolution of the uncertain data can be depicted in the form of a scenario tree, as Fig. 2 shows. The scenario tree consists of nodes and arcs. In the first stage, the root node represents the initial state of the network. In this node, no information has been realized yet, and the decisions should be made without any knowledge. The root node is connected to some nodes (child nodes) in the second stage; each of these nodes is associated with the possible outcomes of the uncertain parameter in this stage. Each of the nodes in the second stage is connected to several nodes in the third stage, which are considered as the possible realization of the uncertain data in the third stage. The branching continues until the final stage. Each unique path for realizing the uncertain date from the first stage to the last stage creates a particular scenario. As illustrated in Fig. 2, each child node is connected to at most one lower-stage node, called the parent node, and the child nodes connected to the same parent node are called sibling nodes. Notably, the stages and periods are not equivalent, and a stage may include several periods.

In a scenario tree, a probability is assigned to each possible realization of the uncertain data. The sum of probabilities associated with sibling nodes equals 1, and the probability of the root node is 1. Moreover, the probability of a scenario is calculated by multiplying the probabilities of the nodes that belong to the unique path associated with that scenario. In the classical MSP, the value of the probabilities is estimated based on the experts' opinions. However, in real-world situations, estimations are subject to uncertainties; therefore, the results may not be reliable in some cases. To address this issue, we apply the MFSP approach, in which the probability of the nodes is considered a fuzzy number. The MFSP approach is presented below, and the definitions are provided in Supplementary Material, Section S1.

4.1. Multi-stage fuzzy stochastic programming approach

In this section, we apply the MFSP approach to the proposed location-allocation model to address the uncertainty in some parameters (the number of suspected cases) and the uncertainty in the probability of the nodes of the scenario tree. The compact form

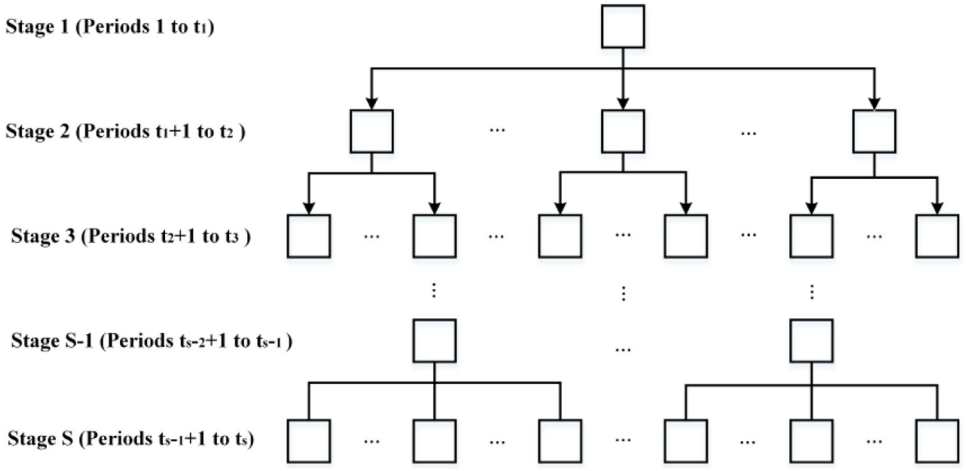

Fig. 2. An illustration of a scenario tree.

of the model is as follows:

$$\begin{aligned} &\min z = \sum_{n\epsilon\mathcal{N}, t\epsilon t_n} \tilde{\mathcal{P}}_n.\eta.x_{tn} \\ &\text{subjectto} \\ &A.x_{tn} \geq \tilde{\alpha}_{tn}, \qquad \forall n\epsilon\mathcal{N},\ t\epsilon t_n \\ &b.u + C.x_{tn} \leq \xi, \qquad \forall n\epsilon\mathcal{N},\ t\epsilon t_n \\ &x_{tn} \geq 0, \quad \forall n\epsilon\mathcal{N},\ t\epsilon t_n;\ u \in \{0,1\} \end{aligned} \tag{50}$$

in which n represents the nodes of the scenario tree ($n\epsilon\mathcal{N}$). $\tilde{\mathcal{P}}_n$ denotes the probability of node n in the scenario tree. This parameter is uncertain, which is considered a triangular fuzzy number. ($\tilde{\mathcal{P}}^n = (\mathcal{P}_n^p, \mathcal{P}_n^m, \mathcal{P}_n^o)$). A and C are the coefficient matrices, and η, b, and ξ are deterministic parameters. x_{tn} corresponds to decision variables, and t_n denotes the periods associated with node n. u is a binary decision variable, which is determined at the beginning of the planning horizon. In fact, it is determined before the realization of any information, and it does not depend on n. $\tilde{\alpha}_{tn}$ is an uncertain parameter, which becomes available in each stage. To deal with the possibilistic objective function and chance constraints, *Me* measure is used, as follows:

$$\begin{aligned} &\min z = E^{Me}\left(\sum_{n\epsilon\mathcal{N}, t\epsilon t_n} \tilde{\mathcal{P}}_n.\eta.x_{tn}\right) \\ &\text{subjectto} \\ &Me\ \{A.x_{tn} \geq \tilde{\alpha}_{tn}\} \geq \Theta, \qquad \forall n\epsilon\mathcal{N},\ t\epsilon t_n \\ &b.u + C.x_{tn} \leq \xi, \qquad \forall n\epsilon\mathcal{N},\ t\epsilon t_n \\ &x_{tn} \geq 0, \quad \forall n\epsilon\mathcal{N},\ t\epsilon t_n;\ u \in \{0,1\} \end{aligned} \tag{51}$$

where Θ is the DMs' minimum confidence level. Formulation (51) can be transformed into *LAM* and *UAM* forms based on Definition S7 (in Supplementary Material). Finally, the deterministic counterparts of *LAM* and *UAM* formulations are provided based on Definitions S5 and S6 and the transformation methods provided in Xu and Zhou (2013) and Zahiri et al. (2017), as shown below.

$$\textbf{\textit{LAM}}: \begin{cases} \min z = E^{Me}\left(\sum_{n\epsilon\mathcal{N}, t\epsilon t_n} \tilde{\mathcal{P}}_n.\eta.x_{tn}\right) \\ \text{subject to} \\ Pos\ \{A.x_{tn} \geq \tilde{\alpha}_{tn}\} \geq \Theta, \qquad \forall n\epsilon\mathcal{N},\ t\epsilon t_n \\ b.u + C.x_{tn} \leq \xi, \qquad \forall n\epsilon\mathcal{N},\ t\epsilon t_n \\ .u + C.x_{tn} \leq \xi, \qquad \forall n\epsilon\mathcal{N},\ t\epsilon t_n \end{cases}$$

$$\textbf{\textit{UAM}}: \begin{cases} \min z = E^{Me}\left(\sum_{n\epsilon\mathcal{N}, t\epsilon t_n} \tilde{\mathcal{P}}_n.\eta.x_{tn}\right) \\ \text{subject to} \\ Nec\ \{A.x_{tn} \geq \tilde{\alpha}_{tn}\} \geq \Theta, \qquad \forall n\epsilon\mathcal{N},\ t\epsilon t_n \\ b.u + C.x_{tn} \leq \xi, \qquad \forall n\epsilon\mathcal{N},\ t\epsilon t_n \\ x_{tn} \geq 0, \quad \forall n\epsilon\mathcal{N},\ t\epsilon t_n;\ u \in \{0,1\} \end{cases} \tag{52}$$

The deterministic counterparts of *LAM* and *UAM* are as follows (Zahiri et al. (2017)):

$$\textbf{\textit{LAM}}: \begin{cases} \min z = \sum_{n\epsilon\mathcal{N}, t\epsilon t_n} \left(\left(\frac{1-\Gamma}{2}\right).\dot{\mathcal{P}}_n^p + \frac{1}{2}.\dot{\mathcal{P}}_n^m + \frac{\Gamma}{2}.\dot{\mathcal{P}}_n^o\right).\eta.x_{tn} \\ \text{subject to} \\ A.x_{tn} \geq \Theta.\alpha_{tn}^m + (1-\Theta).\alpha_{tn}^p, \qquad \forall n\epsilon\mathcal{N},\ t\epsilon t_n \\ b.u + C.x_{tn} \leq \xi, \qquad \forall n\epsilon\mathcal{N},\ t\epsilon t_n \\ x_{tn} \geq 0, \quad \forall n\epsilon\mathcal{N},\ t\epsilon t_n;\ u \in \{0,1\} \end{cases}$$

$$\textbf{\textit{UAM}}: \begin{cases} \min z = \sum_{n\epsilon\mathcal{N}, t\epsilon t_n} \left(\left(\frac{1-\Gamma}{2}\right).\dot{\mathcal{P}}_n^p + \frac{1}{2}.\dot{\mathcal{P}}_n^m + \frac{\Gamma}{2}.\dot{\mathcal{P}}_n^o\right).\eta.x_{tn} \\ \text{subject to} \\ A.x_{tn} \geq (1-\Theta).\alpha_{tn}^m + \Theta.\alpha_{tn}^o, \qquad \forall n\epsilon\mathcal{N},\ t\epsilon t_n \\ b.u + C.x_{tn} \leq \xi, \qquad \forall n\epsilon\mathcal{N},\ t\epsilon t_n \\ x_{tn} \geq 0, \quad \forall n\epsilon\mathcal{N},\ t\epsilon t_n;\ u \in \{0,1\} \end{cases} \tag{53}$$

where Γ is the optimistic-pessimistic parameter of the *Me* measure, as stated in Definition S3. Also, $\dot{\mathcal{P}}_n$ is the updated value of $\mathcal{P}_n$ based on Definition S8. The MFSP form of the proposed model in Section 3.1 and its deterministic counterpart are provided in Supplementary Material, Section S2.

5. The case

On 17 November 2019, the first C-19 case was reported in Wuhan, China, and the virus has spread around the world rapidly. The virus has reached Iran on 19 February 2020, and all the provinces of the country were affected by the virus. Tehran is the most populated city in Iran, and therefore, it is one of the most vulnerable cities to C-19. Tehran has 22 districts, in which district 10 is investigated in this study. 317, 160 people live in this area, and it is the most densely populated district in Tehran. As shown in Fig. 3, district 10 is divided into 17 zones called regions henceforth. The population, area, and density of the regions are inserted in Table S1 in Supplementary Material. We assume that the suspected cases in each region are located in the center of the regions. The candidate locations for SFs, HFs, and QFs are shown in Fig. 3. In Iran, there are 120 laboratories for diagnosis C-19, in which 30,000 tests can be conducted daily. Therefore, the capacity of each SF is considered 250. Based on the data of Mousazadeh et al. (2018), the capacity of HF_2s and HF_3s is considered 620. Notably, a proportion of capacities is assigned to non-C-19 patients in HF_2s and HF_3s. Based on the data of Mousazadeh et al. (2018), on average, 190 persons refers to a hospital in district 10 daily, such that 60%, 20%, 8%, and 12% of them need major services, minor services, special care services, and rehabilitation services, respectively. Minor services, rehabilitation services, and a proportion of

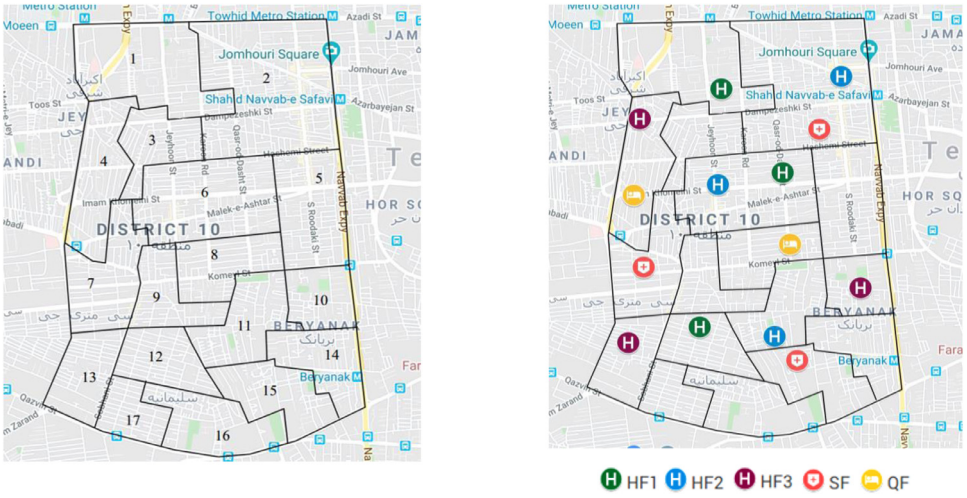

Fig. 3. The regions and the candidate locations of SFs, HFs, and QFs.

major services (such as elective surgeries) can be canceled due to the risk of spreading C-19, and it is supposed that about 60% of the needs for regular services in hospitals declines. Therefore, we consider that the average number of referred non-C-19 cases to a hospital (HF_2 or HF_3) is 76. Besides, the capacities of HF_1s and QFs are considered 500 based on the experts' opinions. The geographical coordinates of the candidate location for SFs, HFs, and QFs are inserted in Table S2. The candidate locations have been chosen so that to be accessible to all people living in this area.

Based on the reports of the Iran ministry of health and medical education, C-19 test results are positive for 25–30% of suspected cases who refer to SFs. 12.3% of these confirmed cases need inpatient care, in which 50% of them have underlying conditions (20% diabetes, 15% hypertension, and 15% cardiovascular disease) (Iran Ministry of Health & Medical Education, 2020). Based on the documented data, a portion of infected patients in HF_2s and HF_3s will die. The death rate of C-19 in Iran is 6% (Worldometers, 2020), in which 90% of them have underlying conditions.[1] Therefore, the death rate in HF_2s and HF_3s is considered 0.6% and 5.4%, respectively. Besides, it is assumed that the discharge rate in HFs and QFs is 50% (Li et al., 2020). Also, it is supposed that the condition of 10% of mild cases will deteriorate, and they will need inpatient care after they are accepted by HF_1s (Chen et al., 2020).

We categorized the population of the area into three age groups: children (0–14), adults (15–64), older adults (above 64). Based on the age-gender pyramid of Tehran, 18%, 73%, and 9% of the population are in the age group 0–14, 15–64, and above 64, respectively (Mean & Median Age of Iranian Population 2016, 2017). The people's susceptibility to C-19 infection varies with the age of the people. Based on the researches, children are less vulnerable to the virus, and the elderly population is the most vulnerable to this virus. In other words, it is declared that the susceptibility to the C-19 tends to increase with age. Therefore, the susceptibility ratio of children to adults is considered 0.34, and the susceptibility ratio of the elderly population to adults is 1.47 (Zhang et al., 2020).

When a C-19 patient coughs, sneezes, or speaks, the susceptible people may be infected by the C-19 virus directly. Furthermore, the objects may be contaminated with the C-19 virus when infected persons touch the objects, which leads to the indirect transmission of the virus. Thus, a transmission event occurs when a susceptible person interacts with infected cases or contaminated objects. We consider that ten transmission events occur hourly according to available data, experts' opinions, and information of the countries that trace C-19 contacts[2,3] (Aleta et al., 2020; Hu et al., 2021). The contact duration for adults is also considered more than for children and older adults since they do a wide range of activities. We also consider that the contact duration of adults with children and elderly groups is higher than with adults because of children and elderly groups' needs for the care of adults.

We calculate the transportation distance between nodes (between the region and SFs, SFs and HFs, HF_1s and HF_2s, HFs and QFs) with Google Maps, and they are reported in Tables S5–S8 (in Supplementary Material). The transportation costs are calculated based on the fuel consumption and distance of the route. Moreover, to calculate the population density of a route connecting two nodes, we first determine the best route between the nodes by Google Map. Then we obtain the portion of the route which is located in each region by Google Map. Finally, we calculate the population density of this route with Formulation 3.

Iran ministry of roads and urban development estimated that cost of construction and equipping a hospital per bed is 131,600$, and consequently, establishing a 600-bed hospital (HF_2 and HF_3) costs 81,592,000$.[4] Also, according to experts' viewpoint, the costs of establishing HF_1 and QFs are estimated at 45,000,000$. The operating cost for a suspected case in SFs is considered 167$.[5] Some C-19 patients will need to stay in the ICU, and C-19 patients with the underlying disease may require treatment in the ICU more than other C-19 patients. 5% of C-19 patients in HF_2s and 20% of C-19 cases in HF_3s are sent to ICUs.[6] The average length of staying at hospitals for C-19 patients who will need intensive care is seven days, and the average length of staying at the hospital for other C-19 patients is five days (Rees et al., 2020). Besides, the cost of treating a mild C-19 patient is 643$, and the cost of treating a severe C-19 patient is 1286$.[7] Accordingly, the daily costs for treating one patient in HF_1, HF_2, and HF_3 are 120$, 130$, and 140$, respectively. Finally, the patients are sent to QFs, and the average length of staying in QFs is seven days.[8] The operating cost in QFs is estimated at 600$ per patient, and consequently, the daily operating

[1] https://tn.ai/2287823

[2] https://www.health.nd.gov/diseases-conditions/coronavirus/north-dakota-coronavirus-cases#collapse-accordion-3661-1

[3] https://www.nj.gov/health/cd/topics/covid2019_dashboard.shtml

[4] https://tn.ai/2109911

[5] https://www.borna.news/fa/tiny/news-1015999

[6] https://www.jjo.ir/005Ile

[7] https://www.eghtesadonline.com/n/2Hhu

[8] https://www.jjo.ir/005Ile

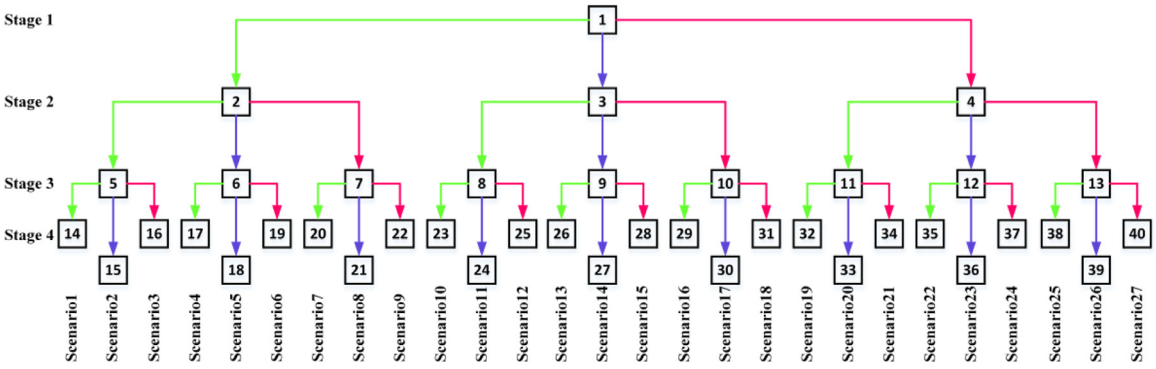

Fig. 4. The scenario tree of the proposed problem.

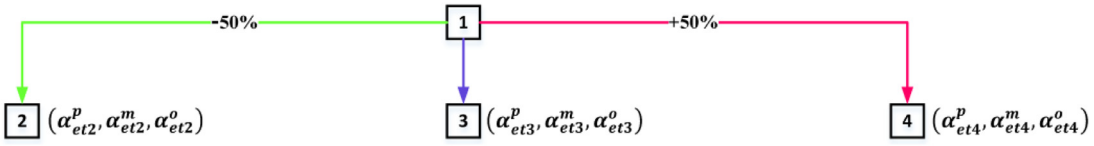

Fig. 5. The relation between the values of the sibling nodes.

cost in QFs per patient is 86$. Moreover, the total budget is considered 600,000,000$ based on the experts' opinion.

The related scenario tree to the proposed problem is depicted in Fig. 4. The scenario tree includes four stages, each of which includes two periods (stage 1 (t_1=1,2), stage 2 (t_2=3,4), stage 3 (t_3=5,6), and stage 4 (t_4=7,8)). The probability of the nodes and their revised values are inserted in Table S3 in Supplementary Material. The probability is determined based on the experts' opinions and regarding the available data. Furthermore, the number of suspected cases in each region and each period associated with each node of the scenario tree ($\tilde{\alpha}_{etn}$) is a fuzzy number, which is determined as $\tilde{\alpha}_{etn} = (\alpha^p_{etn}, \alpha^m_{etn}, \alpha^o_{etn}) = (0.8\alpha^m_{etn}, \alpha^m_{etn}, 1.2\alpha^m_{etn})$. Furthermore, each parent node is connected to three child nodes, as shown in Fig. 4. We consider that among sibling nodes, the number of the suspected cases of the left child node is 50% of the associated value to the middle child node; also, for the right child node, this value is 150% of the associated value to the middle child node. For example, for sibling nodes 2, 3, and 4, we consider that $(\alpha^p_{et2}, \alpha^m_{et2}, \alpha^o_{et2}) = 0.5 \times (\alpha^p_{et3}, \alpha^m_{et3}, \alpha^o_{et3})$ and $(\alpha^p_{et4}, \alpha^m_{et4}, \alpha^o_{et4}) = 1.5 \times (\alpha^p_{et3}, \alpha^m_{et3}, \alpha^o_{et3})$, as shown in Fig. 5. Additional data are provided in the Supplementary Material, Section S3.

6. Implementation and evaluation

In this section, the proposed model is solved using the real data, and the MFSP approach is applied to hedge against uncertainties. All models are solved by GAMS software and Cplex solver in a reasonable time with 0.00% GAP. The results are reported in the following, and analyses are conducted on some important parameters.

6.1. Implementation results

First, we formulate the location-allocation problem. Then, the MFSP approach is applied to the model to cope with uncertain parameters. By applying this approach, the model transforms into *LAM* and *UAM*, which are equivalent to the lower and upper approximation models, respectively. The results of these models suggest interval values for DMs; consequently, DMs can make their decisions in this interval regarding their preferences. In decision-making in fuzzy environments, the MFSP approach provides a range of potential choices for DMs, and the maximum and minimum levels of optimal decisions are determined. Accordingly, DMs can assess the different choices and make the best decisions regarding their attitudes. Based on Definition S7, the feasible region of *LAM* is greater than *UAM*, and consequently, the value of the objective function of *LAM* is lower than *UAM*. The model is solved for $\Gamma = 0.5$ and $\Theta = 0.9$, and the summary of the results is provided in Table 1 and Table B1 (in Appendix B).

The proposed model aims to minimize the transmission rate of the C-19 virus during the planning horizon in district 10 of Tehran by considering different scenarios. Based on Table 1, the objective value of the *LAM* is 0.11154%, and the objective value of the *UAM* is 0.136414%. In fact, the MFSP approach provides the interval solution [0.0011154, 0.00136414] for DMs to make better decisions in the fuzzy environment. The *UAM* is formulated with a more pessimistic attitude than *LAM*, and consequently, the value of the objective function of the *UAM* is greater than the objective value of the *LAM*. Furthermore, the established facilities in the network for *LAM* and *UAM* are determined in Table 1. The number and location of the established SFs and HFs (HF_1s, HF_2s, and HF_3s) are the same for *LAM* and *UAM*. However, by solving *LAM*, two QFs are suggested to be established in the network, and by solving *UAM*, one QF is opened. The reason is that the *UAM* is formulated based on the *Nec* measure, and the number of suspected cases is considered more than that number in *LAM*; consequently, the number of C-19 patients and the cost associated with their treatment increase. As a result, more budget is spent on treating patients, and the number of established QFs decreases (regarding the limited budget). The locations of established facilities are depicted in Fig. 6. Furthermore, it is determined that approximately 80% of the established HF_2s and the HF_3 is assigned to non-C-19 patients. Also, due to the sufficient capacity, no patients have been rejected by health centers (SFs, HFs, and QFs).

The number of suspected cases assigned to SFs and the number of occupied beds by C-19 patients in HFs and QFs during the planning horizon under each scenario are inserted in Table B1 in Appendix B. As mentioned before, the number of PT_1s is greater than the number of PT_2s and PT_3s, and consequently, more beds are occupied in HF_1s rather than HF_2s and HF_3s under each scenario. Besides, despite the same ratio of PT_2s and PT_3S, more beds are occupied in HF_2s than HF_3s under each scenario. The reason

Table 1
The summary of the results for *LAM* and *UAM*.

	TT	U_1^S	U_2^S	U_3^S	U_{11}^H	U_{12}^H	U_{13}^H	U_{21}^H	U_{22}^H	U_{23}^H	U_{31}^H	U_{32}^H	U_{33}^H	U_1^Q	U_2^Q
LAM	0.00111540	0	1	1	1	0	1	1	1	1	0	0	1	1	1
UAM	0.00136414	0	1	1	1	0	1	1	1	1	0	0	1	1	0

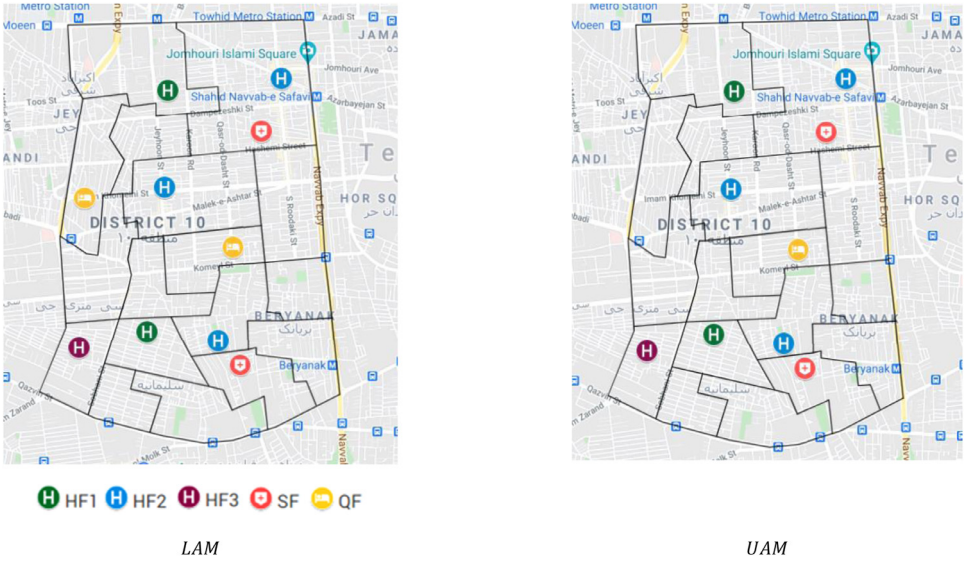

Fig. 6. The locations of established SFs, HFs, and QFs.

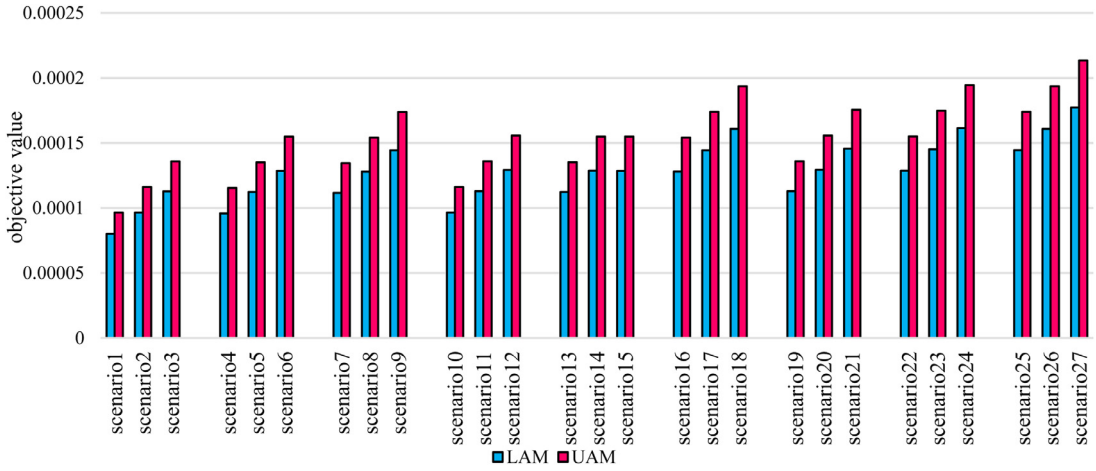

Fig. 7. The value of the transmission rate under each scenario.

is that a portion of PT_1s is transferred from HF_1s to HF_2s due to the deterioration of their conditions. Furthermore, the number of occupied beds in QFs is shown in Table B1, which is less than the number of occupied beds in HFs. Given that the minimum duration of treatment is considered four days, no bed is occupied until the fourth period. On the other hand, the patients admitted to hospitals from the 4th period onwards will be transferred to QFs from the 9th period onwards (regarding the eight-period planning horizon). For these reasons, the number of occupied beds in QFs is low. The transmission rate of the C-19 under each scenario is depicted in Fig. 7. We categorize the scenarios into 9 clusters regarding the optimism degree associated with each leaf node (the nodes with no child nodes) (i.e. (1,2,3), (4,5,6), (7,8,9), (10,11,12), (13,14,15), (16,17,18), (19,20,21), (22,23,24), and (25,26,27)). It is evident that in each cluster, the transmission rate increases from left to right due to decreasing the optimism degree.

In this study, the models are solved using GAMS software with the CPLEX solver for district 10 of Teheran. The models are solved in reasonable times with 0.00% GAP (*LAM*: 42.676 and *UAM*: 83.291 s). All the models run for sensitivity analyses have been completed in less than 5 min with 0.00% GAP. Therefore, using algorithms for solving the models regarding the presented network and collected data is not necessary. However, the model can be applied to larger-scale case studies than district 10 of Teheran, or planning the network may be considered for more time periods. In such cases, the number of continuous and binary variables and the number of constraints increase. The model presented in this study is mixed-integer linear programming (MILP), and the number of binary variables is an important indicator of computational complexity in this model (Alemany et al., 2018; Carrión & Arroyo, 2006; Viana & Pedroso, 2013; Williams, 2013). By increasing the network size, increasing the number of time periods, or increasing both, the number of binary variables and the problem's computa-

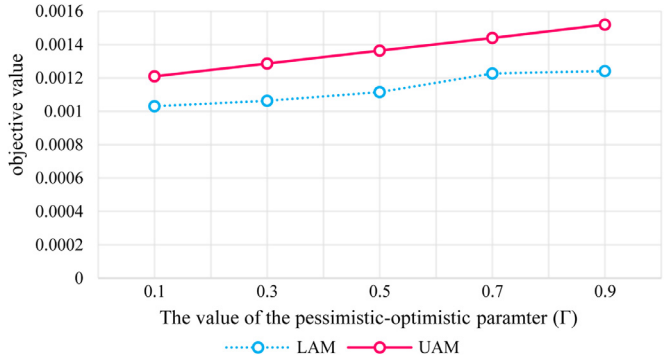

Fig. 8. Objective values versus values of Γ.

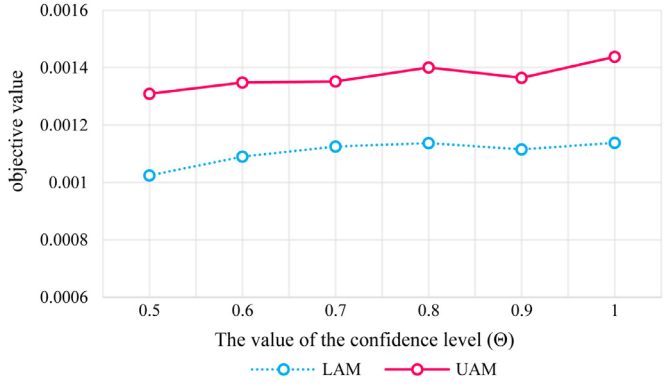

Fig. 9. Objective values versus values of Θ.

tional complexity increase. Therefore, heuristic and metaheuristic techniques can be used to overcome computational difficulties.

6.2. Comparative analysis

The proposed model includes several parameters, and sensitivity analysis is conducted on some important parameters to help DMs obtain better solutions. The variation of the objective values of *LAM* and *UAM* for different values of the optimistic-pessimistic parameter (Γ) is depicted in Fig. 8. In practice, Γ is a pessimistic parameter in minimization problems, and it is considered an optimistic parameter in maximization problems. This study aims to minimize the transmission rate, and the increment of Γ will lead to adopting a more pessimistic attitude in the decision-making process. Therefore, the objective values of *LAM* and *UAM* increase as the value of Γ increases. Thus, DMs can select their ideal optimism-pessimism degree in their decisions, which leads to optimal decisions in an uncertain environment.

The variation of the objective values of *LAM* and *UAM* for different confidence levels (Θ) is depicted in Fig. 9. By increasing the value of the Θ, the feasible region shrinks, and consequently, the objective value increases. When the DMs apply more strict attitudes toward chance constraint, they choose a higher confidence level. As the confidence level increases, the feasible region shrinks, and the objective value increases in the minimization problems. In the proposed model, as the value of Θ increases, the number of the suspected cases increases, and consequently, the transmission rate increases. However, in this problem, by increasing the value of the Θ from 0.8 to 0.9, the objective value decreases. The reason is that by solving the model for $\Theta = \{0.5,\ 0.6,\ 0.7,\ 0.8,\ 1\}$, the same facilities are established (as shown in Table 1), whereas different facilities are established for $\Theta = 0.8$. In this case, the model determines to establish HF_{32} based on the optimal solution. When HF_{32} is opened, the suspected cases should travel longer distances

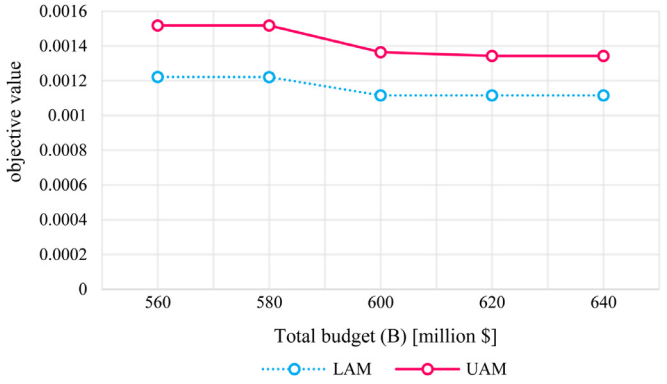

Fig. 10. Objective values versus values of B.

to reach HFs compared to when HF_{33} is established. Therefore, the transmission rate rises further, and consequently, the objective value increases further.

The variation of the objective values of *LAM* and *UAM* for different budget values (B) is depicted in Fig. 10. It is evident that services will be provided for more patients and more efficiently by increasing the budget. For example, the number of established capacities may increase, which makes access to health centers easier. In this case, the traveled distance becomes shorter, and the transmission rate decreases. Also, the shorter route may be crowded in some cases and the possibility of virus transmission increases. In such cases, the model will seek the route for transferring patients to health centers, in which the possibility of the virus transmission is less, even if the route is longer. Accordingly, more transportation costs are imposed, and the transmission rate decreases in a preferable manner.

The variation of the objective values of *LAM* and *UAM* for different values of $\mathbb{N}$ and $\mathbb{T}$ is depicted in Fig. 11. As mentioned before, $\mathbb{N}$ is the average number of transmission events during contact between a C-19 patient and other persons, and $\mathbb{T}$ is the average duration of contact between a C-19 patient and another person. Fig. 11(a) shows that the transmission rate increases by increasing the average number of transmission events. Regarding Formulation (4), $\mathbb{N}$ affects the possibility of the transmission ($\mathbb{P}$), and the possibility increases by the increment of $\mathbb{N}$, leading to an increased transmission rate. In Fig. 11(b), it is observed that the transmission rate increases as the average duration of contacts between a susceptible case and other persons increases. Based on Formulations (2) and (4), $\mathbb{T}$ affects the contact rate ($\mathbb{C}$) and the possibility of transmission, and finally, the transmission rate between a C-19 patient and a susceptible person increases as $\mathbb{T}$ increases; as a result, the total transmission rate increases in the network. In Fig. 11(c) and (d), the effects of simultaneous variations in the values of $\mathbb{N}$ and $\mathbb{T}$ on the objective values are investigated. It is evident that the transmission rate increases exponentially with a simultaneous increase in the value of $\mathbb{N}$ and $\mathbb{T}$. Notably, the objective value of *UAM* is more influenced than the objective value of *LAM* by increasing $\mathbb{N}$ and $\mathbb{T}$. In other words, when the values of $\mathbb{N}$ and $\mathbb{T}$ are smaller, the solution interval is smaller. The interval becomes larger as $\mathbb{N}$ and $\mathbb{T}$ increase. Therefore, for higher values of $\mathbb{N}$ and $\mathbb{T}$, the DMs' opinions significantly affect the obtained results. Fig. 11(d) investigates the effects of the variation in $\mathbb{N}$ and $\mathbb{T}$ if they vary in the opposite direction. It can be said that $\mathbb{T}$ has a greater effect on the transmission rate rather than $\mathbb{N}$. Furthermore, in this chart, the objective value for $(\mathbb{N}, \mathbb{T})$ is greater than the objective value of the other combination of $\mathbb{N}$ and $\mathbb{T}$ (i.e. ($\mathbb{N}$ −40%, $\mathbb{T}$ + 40%), ($\mathbb{N}$ −20%, $\mathbb{T}$ + 20%), ($\mathbb{N}$ +20%, $\mathbb{T}$ − 20%), and ($\mathbb{N}$ +40%, $\mathbb{T}$ − 40%)). In other words, a decrease in one factor ($\mathbb{N}$ or $\mathbb{T}$) has a greater effect on the transmission rate rather than an increase in another.

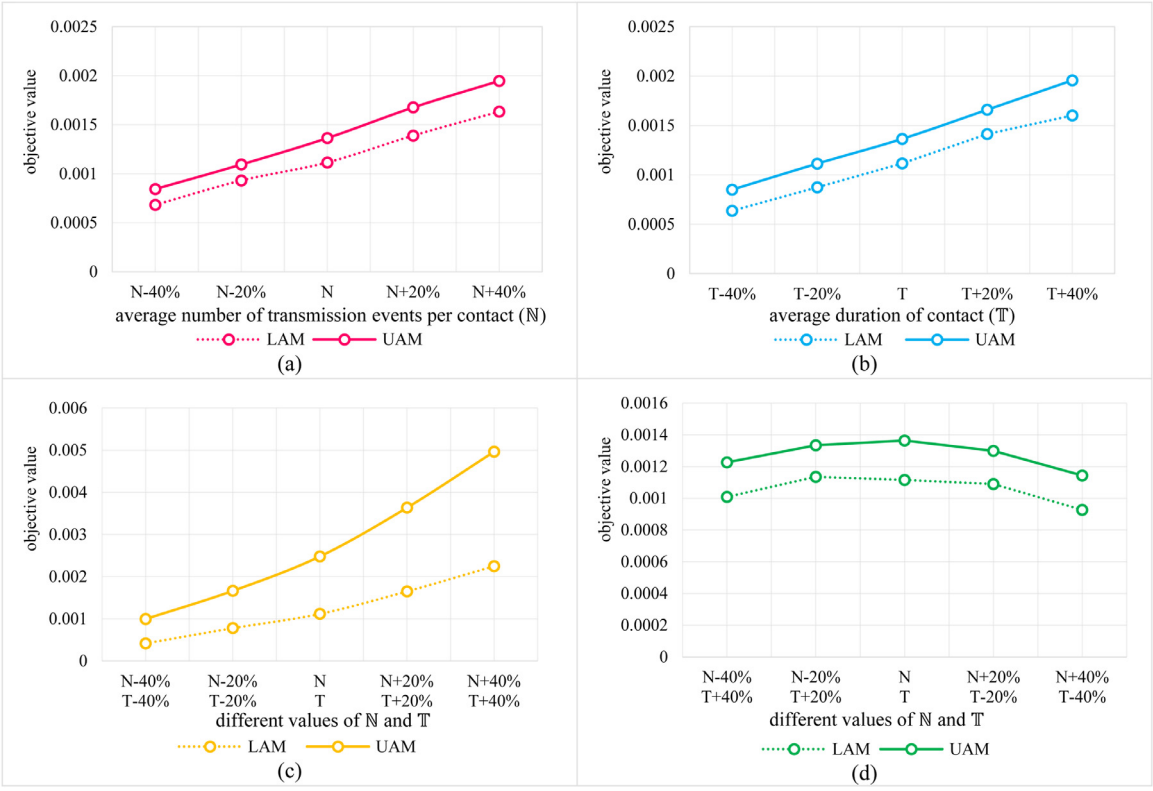

Fig. 11. Objective values versus values of $\mathbb{N}$ and $\mathbb{T}$.

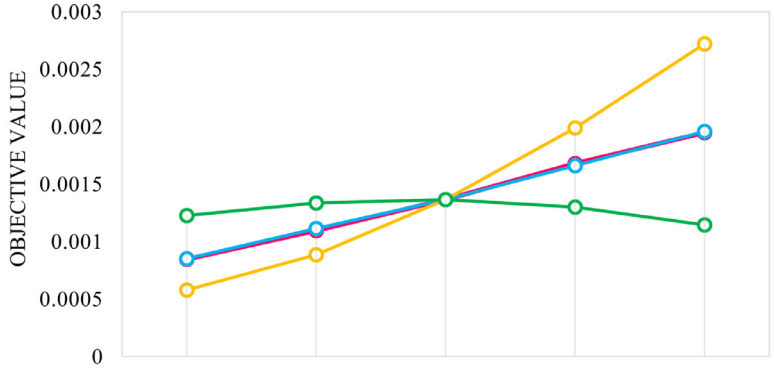

ℕ ↑ 𝕋 ↕		N-40% T	N-20% T	N T	N+20% T	N+40% T
ℕ ↕ 𝕋 ↑		N T-40%	N T-20%	N T	N T+20%	N T+40%
ℕ ↑ 𝕋 ↑		N-40% T-40%	N-20% T-20%	N T	N+20% T+20%	N+40% T+40%
ℕ ↑ 𝕋 ↓		N-40% T+40%	N-20% T+20%	N T	N+20% T-20%	N+40% T-40%

Fig. 12. Objective value for *UAM* versus values of $\mathbb{N}$ and $\mathbb{T}$ (↑: increase, ↑: fixed, ↓: decrease).

In Figs. 12 and 13, the related transmission rates of *LAM* and *UAM* for the different combinations of the values of $\mathbb{N}$ and $\mathbb{T}$ are compared to determine the optimal policies to be adopted. It is evident that when the value of one of these factors ($\mathbb{N}$ and $\mathbb{T}$) is fixed and the other changes, their effects on the transmission rate are approximately the same. Besides, the least impact on the transfer rate is observed when these factors change in opposite directions. On the other hand, we have the most impact on the objective values when co-directional changes are observed in the value of $\mathbb{N}$ and $\mathbb{T}$. Notably, an increase in the values of the factors has a greater influence than a decrease in their values. For example, when the values of the $\mathbb{N}$ and $\mathbb{T}$ increase by 40%, the objective value of *LAM* and *UAM* are doubled approximately. On the other hand, if the values of $\mathbb{N}$ and $\mathbb{T}$ decrease by 40%, the objective values of *LAM* and *UAM* decrease by 60%. Therefore, firstly, it is vital to adopt measures to control the virus transmission as much as possible, and after stabilizing the situations, solutions are sought to reduce the transmission rate.

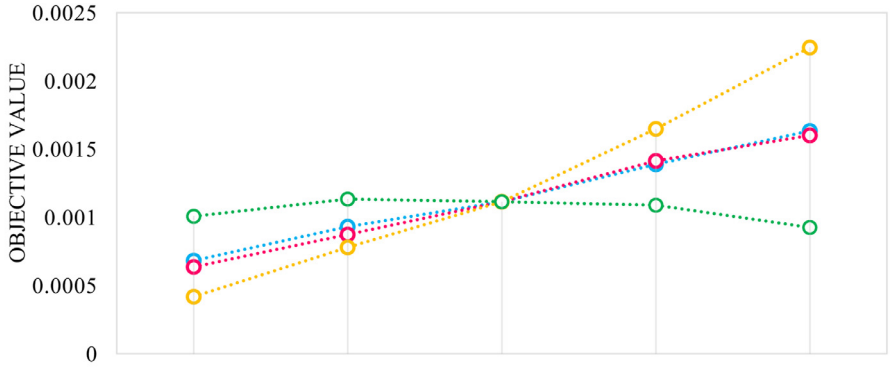

$\mathbb{N}\uparrow\ \mathbb{T}\updownarrow$	····●····	N-40% T	N-20% T	N T	N+20% T	N+40% T
$\mathbb{N}\updownarrow\ \mathbb{T}\uparrow$	····●····	N T-40%	N T-20%	N T	N T+20%	N T+40%
$\mathbb{N}\uparrow\ \mathbb{T}\uparrow$	····●····	N-40% T-40%	N-20% T-20%	N T	N+20% T+20%	N+40% T+40%
$\mathbb{N}\uparrow\ \mathbb{T}\downarrow$	····●····	N-40% T+40%	N-20% T+20%	N T	N+20% T-20%	N+40% T-40%

Fig. 13. Objective value for *LAM* versus values of $\mathbb{N}$ and $\mathbb{T}$ ($\uparrow$: increase, $\uparrow$: fixed, $\downarrow$: decrease).

Wearing face masks and performing respiratory hygiene and hand hygiene can reduce transmission events. Other measures such as teleworking, physical distancing, and avoiding mass gathering can reduce the contact between C-19 cases and susceptible cases. Also, isolation of C-19 cases and quarantine of persons who had contacts with C-19 cases can reduce the contact rate. At the beginning of the CVO, restrictions were imposed in most countries; as a result, the transmission rate decreased, and the situation was stabilized; however, the virus spread was not stopped in most affected countries. In such circumstances, the restrictions were lifted, and most people returned to work due to the economic consequences of CVO. Accordingly, the number of transmission events increases. Now, there are three possibilities regarding people's behavior against C-19: 1) $\mathbb{T}$ will decrease, $\mathbb{N}$ will increase, and the transmission rate will remain constant approximately (regarding the green graph); 2) one of $\mathbb{T}$ and $\mathbb{N}$ will remain constant, the other will increase, and the transmission rate will increase (regarding the pink and blue graphs); 3) $\mathbb{T}$ and $\mathbb{N}$ will increase, and the transmission rate will increase significantly. Therefore, the transmission rate will not decrease much, even in the best conditions. Moreover, according to these graphs, it is concluded that the impact of $\mathbb{N}$ and $\mathbb{T}$ on the transmission rate are the same.

The vaccine is another effective tool for controlling infectious disease transmission (Duijzer et al., 2018; Lin et al. 2020). The studies showed that the viral load of the C-19 virus in vaccinated patients is approximately one-third of that of unvaccinated patients (Levine-Tiefenbrun et al., 2021; Vitiello et al., 2021). This factor reduces people's susceptibility to C-19 infection ($\mathbb{S}_g$) accordingly. We show the decreased susceptibility to C-19 infection by $\mathbb{S}'_g$. Regarding those as mentioned earlier, the share of vaccinated and unvaccinated populations affects the transmission rate. In Fig. 14, we investigate the impact of the different shares of vaccinated populations on the transmission rate. To do so, we calculate the new value of $\mathbb{S}_g$ ($\mathbb{S}''_g$) for ipercent of the vaccinated population as follows:

$$\mathbb{S}''_g = \mathbb{S}_g.(1-\mathrm{i}) + \mathbb{S}'_g.i \tag{54}$$

As shown in Fig. 14, the transmission rate decreases significantly as the share of the vaccinated population increases. This figure shows that If people in an unvaccinated area are supposed to

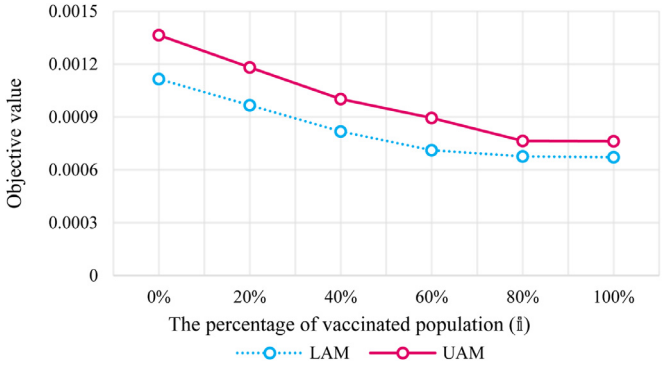

Fig. 14. Objective values versus share of the vaccinated population.

be fully vaccinated immediately, the transmission rate in that area will be reduced by 50%. Therefore, if proper vaccination policy had been adopted and at least a part of the population had been vaccinated, we would have witnessed a lower transmission rate. The effect of time is not considered here, and it is assumed that a part of the population will be vaccinated immediately. For this reason, with the complete vaccination of the population, the transmission rate has not reached zero. However, it is observed that after vaccination of 80% of the population, the transmission rate reaches relative stability. Therefore, it is concluded that at least 80% of people need to be vaccinated to reach a relatively stable immunity against C-19.

When COVID-19 patients are transporting, they are under the control of healthcare staff and are provided with better protection. The better the protection, the less the number of transmission events. As a result, different degrees of protection influence the possibility of transmission to others, and consequently, the transmission rate of COVID-19. In Fig. 15, we investigate the impact of different protection degrees on the transmission rate. Better protection reduces the number of transmission events ($\mathbb{N}$). We consider four protection degrees: when protection is *sufficient*, in which case the number of transmission events is $\mathbb{N}$, when protection is *good*, in which case the number of transmission events is

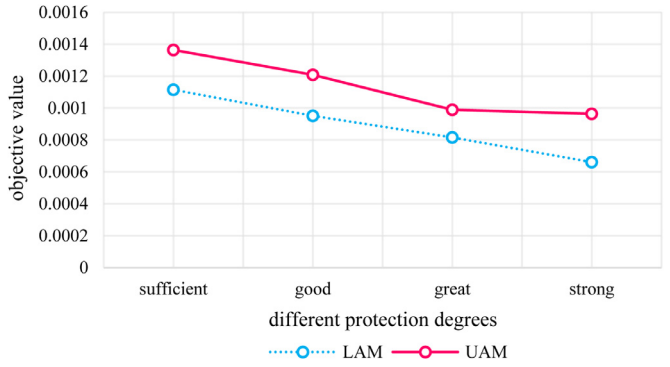

Fig. 15. Objective values versus protection degrees.

reduced by 25% (0.75$\mathbb{N}$), when protection is *great*, in which case the number of transmission events is reduced by 50% (0.5$\mathbb{N}$), and when protection is *strong*, in which case the number of transmission events reduced by 75% (0.25$\mathbb{N}$). Notably, this protection is provided with healthcare staff, and therefore, this protection does not affect the transmission of the virus when patients move from regions to SFs ($\eta_{ei}^{''RS}$). Besides, the rate of transmission by patients whom hospitals have rejected is not affected by the different degrees of protection that staff provide to patients ($\eta_{e}^{''R}$). Fig. 15 indicates that as the degree of protection for patients increases, the virus transmission rate decreases. Therefore, healthcare staff can also help reduce the transmission rate and contain the outbreak by providing better patient protection.

The people's susceptibility to the C-19 virus varies based on the people's age, and consequently, the population's age structure affects the transmission rate of the C-19 virus. We categorize the susceptible cases into three age groups: children (0–14 years old), adults (15–64 years old), older adults (more than 64 years old), which make up 18%, 73%, and 9% of the population of the studied case. The susceptibility of older adults to C-19 cases is higher than adults (1.47:1). On the other hand, children are less susceptible to the virus than adults (0.34:1). In Fig. 16, the effect of older population size on the transmission rate is investigated. In Fig. 16(a), the population of adults remains constant, and the population size of older adults and children varies. It is evident that the transmission rate of the C-19 increases as the size of the older population increases and the size of the child population decreases.

Similarly, in Fig. 16(b), the transmission rate increases as the number of older people increases and the number of adults decreases, while the number of children remains constant. The reason is that older people are more susceptible to the C-19 virus, which increases the probability of the virus transmission based on Formulation 1; accordingly, by increasing the number of older people that increases the probability of transmitting the virus, the transmission rate rises. It is concluded that policy-makers should tighten restrictions in the area with a large portion of older people to prevent further transmission of the C-19 virus.

The age profile of the population affects the transmission rate of the C-19 virus. Besides, the susceptibility of each age group to the virus affects the optimal solution of the model. The optimal interval solution of the proposed model is [0.0011154, 0.00136414]. The optimal solution without considering the population's age structure is [0.0011293, 0.00133021], which is not a reliable solution. Therefore, taking these issues into account helps DMs to make more reliable decisions during the CVO. In Fig. 17, the sensitivity of the transmission rate to the degree of susceptibility to the C-19 virus is investigated. In Fig. 17(a), the impact of the susceptibility degree of older people on the transmission rate is investigated. In Fig. 17(b), the effect of the susceptibility degree of the child population on the objective values is depicted. It is evident that the transmission rate increases by increasing the susceptibility degree. Besides, increasing the value of $\mathbb{S}_{\text{older population}}$ has a greater influence on the objective value than increasing the value of the $\mathbb{S}_{\text{child population}}$. The reason is that the susceptibility of older people is much more than the child population (1.47:034), and consequently, and its changes have a more significant impact on the objective value. Notably, in the studied case, the size of the older population is half the size of the child population; however, the impact of the variation in the value $\mathbb{S}_{\text{older population}}$ is greater on the objective value. Therefore, to obtain more reliable solutions, considering the population's age structure in the decision-making process is of great significance. It can also be said that older people are at high risk of C-19 disease, and the adopted policies should protect them against C-19 effectively.

6.3. The robustness of the MFSP approach

In this section, the robustness of the proposed MFSP approach and the classical MFSP approach are compared. In the classical MFSP, the probabilities of nodes are deterministic, while the probabilities in the proposed MFSP are uncertain and are considered as fuzzy numbers ($\tilde{\mathcal{P}}_n$). The compact form of the proposed MFSP model is considered as follows:

$$\begin{aligned} &\min z = \tilde{\mathcal{P}}.x \\ &\text{subjectto} \\ &A.x \geq \tilde{\alpha} \\ &b.u + C.x \leq \xi \\ &x \geq 0,\ \ u \in \{0,1\} \end{aligned} \tag{55}$$

where $\tilde{\alpha}$ and $\tilde{\mathcal{P}}$ are triangular fuzzy numbers. First, we generate the uncertain parameters randomly in their related fuzzy intervals and solve the model regarding the realized random parameters. Then, the obtained optimal solution (x^*, u^*) under each realization is fixed in the model, and the model is reformulated as follows:

$$\begin{aligned} &\min z = \dot{\mathcal{P}}_{real}.x^* + \Pi.\mathrm{h} + \Pi'.\mathrm{h}' \\ &\text{subjectto} \\ &A.x^* + h \geq \alpha_{real} \\ &b.u^* + C.x^* - h' \leq \xi \\ &h, h' \geq 0 \end{aligned} \tag{56}$$

h and h' represent the violations in the constraints, which are penalized by Π and Π', respectively. Also, $\dot{\mathcal{P}}_{real}$ is the updated value of $\mathcal{P}_{real}$. In Table 2, the total deviation of the proposed MFSP approach and the classical MFSP approach are compared. The value of the confidence level in both approaches is 0.9. It is evident that the proposed MFSP approach avoids constraint violation more than the classical approach. Therefore, the proposed approach outperforms the classical MFSP approach in terms of average violations and the standard deviation of violations. Consequently, it can be said that the constraints are less likely to be violated under each scenario by applying the MFSP approach. According to the above, applying the proposed MFSP approach to the presented model is justified and valid.

7. Conclusion

The novelty of the C-19 virus and the uncertainty that pervades the healthcare systems during the CVO highlight the need for an efficient response to C-19. Besides, deciding on allocating limited available resources becomes more complicated in such circumstances. In this study, a location-allocation model is proposed to obtain an optimized allocation of available resources to C-19 patients while the transmission rate of the C-19 virus minimizes. The susceptibility to C-19 various is an age-dependent factor, and accordingly, different age groups are considered. To calculate the

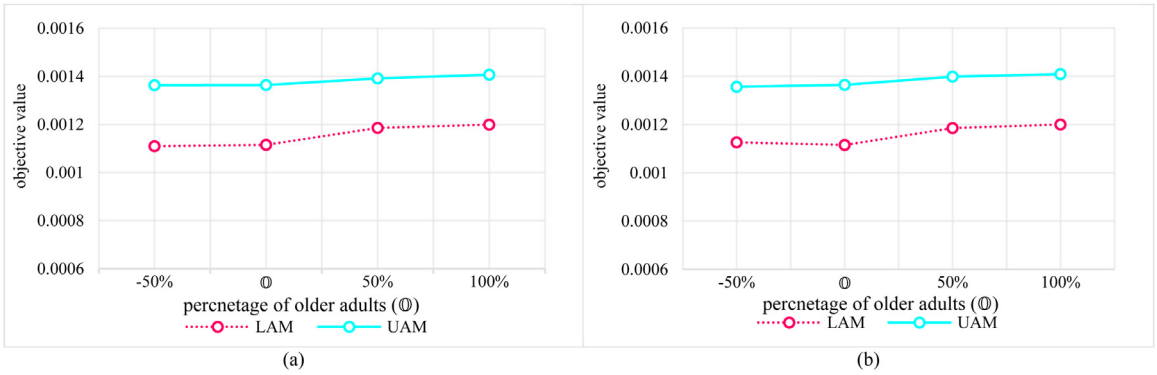

Fig. 16. Objective values versus proportion of older people.

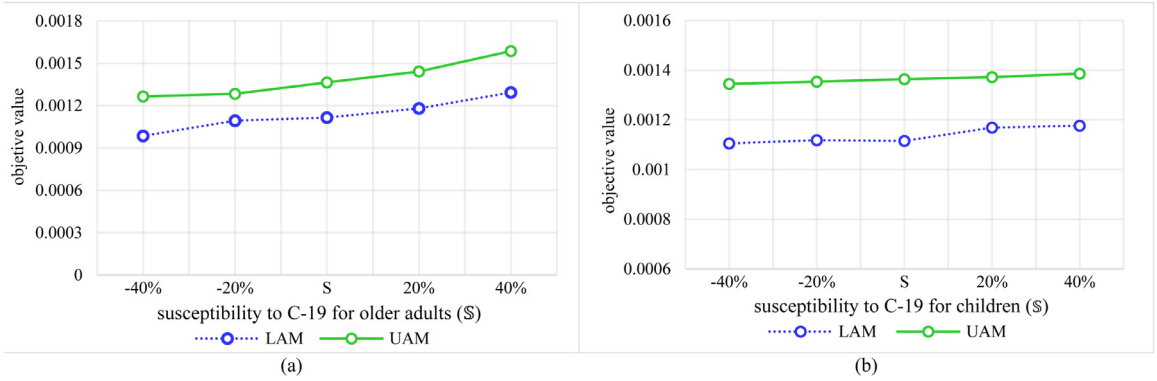

Fig. 17. Objective values versus degree of susceptibility.

Table 2
The total violations of constraints under different realizations.

No. of realization	Classical MFSP *LAM*	*UAM*	Proposed MFSP *LAM*	*UAM*
1	147.83	2001.57	118.45	2000.43
2	139.92	2009.81	136.63	2013.83
3	136.85	2057.18	126.46	2003.40
4	132.31	2001.45	123.51	1973.01
5	148.33	1984.86	139.08	1946.00
6	126.50	2062.50	135.01	1992.16
7	149.77	2023.23	130.13	2001.72
8	129.64	2032.61	132.60	1950.20
9	128.93	2009.49	126.25	2009.27
10	139.13	2033.14	131.05	1999.56
Average	137.92	2021.58	129.92	1988.96
Standard deviation	8.60	25.03	6.34	24.17

rate of the C-19 transmission from a C-19 patient to a susceptible case of a specific age group, a function is developed based on the contact rate, the degree of susceptibility to the C-19 associated with the age group, the probability of disease transmission, and the portion of infected cases. Furthermore, to improve the utilization of limited resources, C-19 patients are categorized into different groups according to their disease severity and are assigned to appropriate HFs to receive medical care tailored to their needs.

Some data are tainted with uncertainty in the proposed model, and the MFSP approach is used to cope with uncertainty. In this approach, the probability of nodes of the scenario tree and the number of suspected cases are treated as fuzzy variables. The *Me* measure is used to cope with chance constraints and the fuzzy objective. By applying this approach, the proposed model is converted into two models, *LAM* and *UAM*, which are based on *Pos* and *Nec* measures, respectively. Finally, the model is applied to the real case, district 10 of Tehran; the results are provided, and sensitivity analyses are carried out, which lead to the following managerial insights:

(1) An interval solution is provided for DMs by applying the proposed MFSP approach, which supplies them with more information. DMs can also incorporate their attitudes into decision-making, which leads to optimal decisions in a fuzzy environment.
(2) The number of transmission events per contact ($\mathbb{N}$) and the average duration of the contact ($\mathbb{T}$) are important factors that affect the transmission rate of the C-19. If the preventive measure is taken in such a way that can decrease the values of $\mathbb{N}$ and $\mathbb{T}$, the transmission rate decreases significantly. However, if the measures can reduce the value of one of these factors and cannot affect the value of the other, a smaller impact on the transmission rate is observed. Besides, if the values of $\mathbb{N}$ and $\mathbb{T}$ change in the opposite direction, the transmission rate remains almost constant.

(3) The vaccine is another effective tool for controlling CVO, and adopting appropriate policies to vaccinate people as soon as possible is very effective in reducing the spread of C-19. Besides, vaccinating at least 80% of the population provides relatively stable immunity against C-19.
(4) The population's age structure affects the transmission rate of C-19, and the older population has a greater influence on the transmission rate. Thus, preventive measures should be taken in such a way that they protect older people against C-19 efficiently and fairly.
(5) By assigning patients to centers providing the services tailored to their needs, the limited resources will be allocated equitably, and the capacity shortage is avoided as much as possible.

As further extensions of this study, the effect of different preventive measures on the transmission rate can be considered. Furthermore, considering the asymptomatically infected cases can make the model more reliable. The uncertainty in the death rate and discharge rate can be taken into account. After assigning different types of C-19 patients to different types of HFs, the patients need different types of medical care according to their disease severity; consequently, the resource allocation within HFs can be incorporated into the model. Moreover, the concept of robustness can be incorporated into the model to improve its performance. Regarding the different viral loads of vaccinated and unvaccinated patients, we can categorize the infected cases into two groups (vaccinated C-19 patients and unvaccinated C-19 patients), which leads to a more accurate transmission rate. (Eqs. (3), (7), (40–50), (52–56) (Table B1)

Supplementary Material: The supplementary material related to this paper can be found in the online version.

Declaration of Competing Interest

The authors declare that they have no conflict of interest.

Supplementary materials

Supplementary material associated with this article can be found, in the online version, at doi:10.1016/j.ejor.2021.11.016.

References

Mean and Median Age of Iranian Population 2016. (2017). Statistical center of Iran. https://www.amar.org.ir/Portals/1/News/files/MeanandMedianAgeofIranianPopulation.pdf
Iran Ministry of Health and Medical Education. (2020). http://corona.behdasht.gov.ir/
Centers for Disease Control and Prevention. (2020). https://www.cdc.gov/coronavirus/2019-ncov/hcp/clinical-guidance-management-patients.html
Abbasi, B., Fadaki, M., Kokshagina, O., Saeed, N., & Chhetri, P. (2020). Modeling vaccine allocations in the COVID-19 pandemic: A case study in Australia. *SSRN Electronic Journal*. https://doi.org/10.2139/SSRN.3744520.
Alam, S. T., Ahmed, S., Ali, S. M., Sarker, S., Kabir, G., & ul-Islam, A. (2021). Challenges to COVID-19 vaccine supply chain: Implications for sustainable development goals. *International Journal of Production Economics, 239*, Article 108193. https://doi.org/10.1016/J.IJPE.2021.108193.
Alemany, J., Kasprzyk, L., & Magnago, F. (2018). Effects of binary variables in mixed integer linear programming based unit commitment in large-scale electricity markets. *Electric Power Systems Research, 160*, 429–438. https://doi.org/10.1016/J.EPSR.2018.03.019.
Aleta, A., Martín-Corral, D., Bakker, M. A., Piontti, A. P., Ajelli, M., Litvinova, M., et al. (2020). Quantifying the importance and location of SARS-CoV-2 transmission events in large metropolitan areas. *MedRxiv* 2020.12.15.20248273. https://doi.org/10.1101/2020.12.15.20248273.
Anparasan, A. A., & Lejeune, M. A. (2018). Data laboratory for supply chain response models during epidemic outbreaks. *Annals of Operations Research, 270*(1–2), 53–64. https://doi.org/10.1007/s10479-017-2462-y.
Carrión, M., & Arroyo, J. M. (2006). A computationally efficient mixed-integer linear formulation for the thermal unit commitment problem. *IEEE Transactions on Power Systems, 21*(3), 1371–1378. https://doi.org/10.1109/TPWRS.2006.876672.
Chen, X., Li, M., Simchi-Levi, D., & Zhao, T. (2020). Allocation of COVID-19 vaccines under limited supply. *MedRxiv* 2020.08.23.20179820. https://doi.org/10.1101/2020.08.23.20179820.
Chowell, G., & Nishiura, H. (2014). Transmission dynamics and control of Ebola virus disease (EVD): A review. *BMC Medicine, 12*(1), 196. https://doi.org/10.1186/s12916-014-0196-0.
Das, T. K., Savachkin, A., & Zhu, Y. (2008). A large-scale simulation model of pandemic influenza outbreaks for development of dynamic mitigation strategies. *IIE Transactions (Institute of Industrial Engineers), 40*(9), 893–905. https://doi.org/10.1080/07408170802165856.
Dasaklis, T. K., Pappis, C. P., & Rachaniotis, N. P. (2012). Epidemics control and logistics operations: A review. *International Journal of Production Economics, 139*(2), 393–410. https://doi.org/10.1016/j.ijpe.2012.05.023.
Dasaklis, T. K., Rachaniotis, N., & Pappis, C. (2017). Emergency supply chain management for controlling a smallpox outbreak: The case for regional mass vaccination. *International Journal of Systems Science: Operations and Logistics, 4*(1), 27–40. https://doi.org/10.1080/23302674.2015.1126379.
Davies, N. G., Klepac, P., Liu, Y., Prem, K., Jit, M., & Eggo, R. M.Group, C. C.-19 working. (2020). Age-dependent effects in the transmission and control of COVID-19 epidemics. *MedRxiv*.
Del Valle, S. Y., Hyman, J. M., & Chitnis, N. (2013). Mathematical models of contact patterns between age groups for predicting the spread of infectious diseases. *Mathematical Biosciences and Engineering: MBE, 10*, 1475.
Dimitrov, N. B., & Meyers, L. A. (2014). Mathematical approaches to infectious disease prediction and control. *INFORMS TutORials in Operations Research*, 1–25. https://doi.org/10.1287/educ.1100.0075.
Duijzer, L. E., van Jaarsveld, W., & Dekker, R. (2018). Literature review: The vaccine supply chain. *European Journal of Operational Research, 268*(1), 174–192. https://doi.org/10.1016/J.EJOR.2018.01.015.
Ekici, A., Keskinocak, P., & Swann, J. L. (2014). Modeling influenza pandemic and planning food distribution. *Manufacturing and Service Operations Management, 16*(1), 11–27. https://doi.org/10.1287/msom.2013.0460.
Georgiadis, G. P., & Georgiadis, M. C. (2021). Optimal planning of the COVID-19 vaccine supply chain. *Vaccine, 39*(37), 5302–5312. https://doi.org/10.1016/J.VACCINE.2021.07.068.
Govindan, K., Mina, H., & Alavi, B. (2020). A decision support system for demand management in healthcare supply chains considering the epidemic outbreaks: A case study of coronavirus disease 2019 (COVID-19). *Transportation Research. Part E, Logistics and Transportation Review, 138*, Article 101967. https://doi.org/10.1016/j.tre.2020.101967.
Hackl, J., & Dubernet, T. (2019). Epidemic spreading in urban areas using agent-based transportation models. *Future Internet, 11*(4), 92. https://doi.org/10.3390/FI11040092.
He, Y., & Liu, N. (2015). Methodology of emergency medical logistics for public health emergencies. *Transportation Research Part E: Logistics and Transportation Review, 79*, 178–200. https://doi.org/10.1016/j.tre.2015.04.007.
Heesterbeek, J. A. P., & Metz, J. A. J. (1993). The saturating contact rate in marriage- and epidemic models. *Journal of Mathematical Biology, 31*(5), 529–539. https://doi.org/10.1007/BF00173891.
Hosseini-Motlagh, S. M., Samani, M. R. G., & Homaei, S. (2020). Toward a coordination of inventory and distribution schedules for blood in disasters. *Socio-Economic Planning Sciences, 100897*. https://doi.org/10.1016/j.seps.2020.100897.
Hu, S., Wang, W., Wang, Y., Litvinova, M., Luo, K., Ren, L., et al. (2021). Infectivity, susceptibility, and risk factors associated with SARS-CoV-2 transmission under intensive contact tracing in Hunan, China. *Nature Communications, 12*(1), 1–11 2021 12:1. https://doi.org/10.1038/s41467-021-21710-6.
Ivanov, D. (2020). Predicting the impacts of epidemic outbreaks on global supply chains: A simulation-based analysis on the coronavirus outbreak (COVID-19/SARS-CoV-2) case. *Transportation Research Part E: Logistics and Transportation Review, 136*, Article 101922. https://doi.org/10.1016/j.tre.2020.101922.
Keeling, M. J., & Eames, K. T. D. (2005). Networks and epidemic models. *Journal of the Royal Society Interface, 2*(4), 295–307.
Koyuncu, M., & Erol, R. (2010). Optimal resource allocation model to mitigate the impact of pandemic influenza: A case study for Turkey. *Journal of Medical Systems, 34*(1), 61–70. https://doi.org/10.1007/s10916-008-9216-y.
Levine-Tiefenbrun, M., Yelin, I., Katz, R., Herzel, E., Golan, Z., Schreiber, L., et al. (2021). Initial report of decreased SARS-CoV-2 viral load after inoculation with the BNT162b2 vaccine. *Nature Medicine, 27*(5), 790–792 2021 27:5. https://doi.org/10.1038/s41591-021-01316-7.
Li, L., Huang, T., Wang, Y., Wang, Z., Liang, Y., Huang, T., et al. (2020). COVID-19 patients' clinical characteristics, discharge rate, and fatality rate of meta-analysis. *Journal of Medical Virology, 92*(6), 577–583. https://doi.org/10.1002/jmv.25757.
Li, Y., Chen, K., Collignon, S., & Ivanov, D. (2021). Ripple effect in the supply chain network: Forward and backward disruption propagation, network health and firm vulnerability. *European Journal of Operational Research, 291*(3), 1117–1131. https://doi.org/10.1016/j.ejor.2020.09.053.
Lin, Qi, Zhao, Q., & Lev, B. (2020). Cold chain transportation decision in the vaccine supply chain. *European Journal of Operational Research, 283*(1), 182–195. https://doi.org/10.1016/J.EJOR.2019.11.005.
Lin, Q., Zhao, S., Gao, D., Lou, Y., Yang, S., Musa, S.S. et al. (2020). A conceptual model for the coronavirus disease 2019 (COVID-19) outbreak in Wuhan, China with individual reaction and governmental action. 10.1016/j.ijid.2020.02.058
Liu, M., Xu, X., Cao, J., & Zhang, D. (2020a). Integrated planning for public health emergencies: A modified model for controlling H1N1 pandemic. *Journal of the Operational Research Society, 71*(5), 748–761. https://doi.org/10.1080/01605682.2019.1582589.
Liu, M., & Zhang, D. (2016). A dynamic logistics model for medical resources allocation in an epidemic control with demand forecast updating. *Journal of the Operational Research Society, 67*(6), 841–852. https://doi.org/10.1057/jors.2015.105.

Liu, Y., Yan, L. M., Wan, L., Xiang, T. X., Le, A., Liu, J. M., et al. (2020b). Viral dynamics in mild and severe cases of COVID-19, *The lancet infectious diseases* (20, pp. 656–657). Lancet Publishing Group. https://doi.org/10.1016/S1473-3099(20)30232-2.

Mehrotra, S., Rahimian, H., Barah, M., Luo, F., & Schantz, K. (2020). A model of supply-chain decisions for resource sharing with an application to ventilator allocation to combat COVID-19. *Naval Research Logistics (NRL), 67*(5), 303–320. https://doi.org/10.1002/nav.21905.

Mousazadeh, M., Torabi, S. A., Pishvaee, M. S., & Abolhassani, F. (2018). Health service network design: A robust possibilistic approach. *International Transactions in Operational Research, 25*(1), 337–373. https://doi.org/10.1111/itor.12417.

Nagurney, A. (2021). Supply chain game theory network modeling under labor constraints: Applications to the Covid-19 pandemic. *European Journal of Operational Research, 293*(3), 880–891. https://doi.org/10.1016/j.ejor.2020.12.054.

Nikolopoulos, K., Punia, S., Schäfers, A., Tsinopoulos, C., & Vasilakis, C. (2021). Forecasting and planning during a pandemic: COVID-19 growth rates, supply chain disruptions, and governmental decisions. *European Journal of Operational Research, 290*(1), 99–115. https://doi.org/10.1016/j.ejor.2020.08.001.

Nkengasong, J. (2020). China's response to a novel coronavirus stands in stark contrast to the 2002 SARS outbreak response. *Nature Medicine, 26*(3), 310–311. https://doi.org/10.1038/s41591-020-0771-1.

Pandey, A., Atkins, K. E., Medlock, J., Wenzel, N., Townsend, J. P., & Childs, J. E. (2014). Strategies for containing Ebola in West Africa. *Science, 346*(6212), 991–995 (New York, N.Y.). https://doi.org/10.1126/science.1260612.

Peirlinck, M., Linka, K., Sahli Costabal, F., & Kuhl, E. (2020). Outbreak dynamics of COVID-19 in China and the United States. *Biomechanics and Modeling in Mechanobiology*, 1–15. https://doi.org/10.1007/s10237-020-01332-5.

Psarris, P., & Floudas, C. A. (1990). Improving dynamic operability in mimo systems with time delays. *Chemical Engineering Science, 45*(12), 3505–3524. https://doi.org/10.1016/0009-2509(90)87155-L.

Rachaniotis, N. P., Dasaklis, T. K., & Pappis, C. P. (2012). A deterministic resource scheduling model in epidemic control: A case study. *European Journal of Operational Research, 216*(1), 225–231. https://doi.org/10.1016/j.ejor.2011.07.009.

Rees, E. M., Nightingale, E. S., Jafari, Y., Waterlow, N., Clifford, S., Group, C. W., et al. (2020). COVID-19 length of hospital stay: A systematic review and data synthesis. *MedRxiv*. https://doi.org/10.1101/2020.04.30.20084780.

Ren, Y., Órdoñez, F., & Wu, S. (2013). Optimal resource allocation response to a smallpox outbreak. *Computers and Industrial Engineering, 66*(2), 325–337. https://doi.org/10.1016/j.cie.2013.07.002.

Roberts, M. G. (1996). The dynamics of bovine tuberculosis in possum populations, and its eradication or control by culling or vaccination. *The Journal of Animal Ecology, 65*(4), 451. https://doi.org/10.2307/5780.

Samani, M. R. G., Hosseini-Motlagh, S. M., & Homaei, S. (2020). A reactive phase against disruptions for designing a proactive platelet supply network. *Transportation Research Part E: Logistics and Transportation Review, 140*, Article 102008. https://doi.org/10.1016/j.tre.2020.102008.

Silal, S. P. (2021). Operational research: A multidisciplinary approach for the management of infectious disease in a global context. *European Journal of Operational Research, 291*(3), 929–934. https://doi.org/10.1016/j.ejor.2020.07.037.

Sinha, P., Kumar, S., & Chandra, C. (2021). Strategies for ensuring required service level for COVID-19 herd immunity in Indian vaccine supply chain. *European Journal of Operational Research*. https://doi.org/10.1016/J.EJOR.2021.03.030.

Tanner, M. W., & Ntaimo, L. (2010). IIS branch-and-cut for joint chance-constrained stochastic programs and application to optimal vaccine allocation. *European Journal of Operational Research, 207*(1), 290–296. https://doi.org/10.1016/j.ejor.2010.04.019.

Tebbens, R. J. D., & Thompson, K. M. (2009). Priority shifting and the dynamics of managing eradicable infectious diseases. *Management Science, 55*(4), 650–663. https://doi.org/10.1287/mnsc.1080.0965.

Viana, A., & Pedroso, J. P. (2013). A new MILP-based approach for unit commitment in power production planning. *International Journal of Electrical Power & Energy Systems, 44*(1), 997–1005. https://doi.org/10.1016/J.IJEPES.2012.08.046.

Vitiello, A., Ferrara, F., Troiano, V., & Porta, R. La (2021). COVID-19 vaccines and decreased transmission of SARS-CoV-2. *Inflammopharmacology, 1*. https://doi.org/10.1007/S10787-021-00847-2.

Wanying, C., Alain, G., & Angel, R. (2016). Modeling the logistics response to a bioterrorist anthrax attack. *European Journal of Operational Research, 254*(2), 458–471. https://doi.org/10.1016/j.ejor.2016.03.052.

Weissman, G. E., Crane-Droesch, A., Chivers, C., Luong, T., Hanish, A., & Levy, M. Z. (2020). Locally informed simulation to predict hospital capacity needs during the COVID-19 pandemic. *Annals of Internal Medicine, 173*(1), 21–28. https://doi.org/10.7326/M20-1260.

WHO. (2020a). *Critical preparedness, readiness and response actions for COVID-19: Interim guidance, 22 march 2020*. World Health Organization.

WHO. (2020b). *Operational considerations for case management of COVID-19 in health facility and community: Interim guidance, 19 march 2020*. World Health Organization.

Williams, H. P. (2013). *Model building in mathematical programming*. John Wiley & Sons.

Worldometers. (2020). https://www.worldometers.info/coronavirus/, Date Accessed: 2020-05-01

Worldometers. (2021). https://www.worldometers.info/coronavirus/, Date Accessed: 2021-06-12.

Xu, J., & Zhou, X. (2013). Approximation based fuzzy multi-objective models with expected objectives and chance constraints : Application to earth-rock work allocation. *Information Sciences, 238*, 75–95. https://doi.org/10.1016/j.ins.2013.02.011.

Yarmand, H., Ivy, J. S., Denton, B., & Lloyd, A. L. (2014). Optimal two-phase vaccine allocation to geographically different regions under uncertainty. *European Journal of Operational Research, 233*(1), 208–219. https://doi.org/10.1016/j.ejor.2013.08.027.

Zahiri, B., Torabi, S. A., & Tavakkoli-moghaddam, R. (2017). A novel multi-stage possibilistic stochastic programming approach (with an application in relief distribution planning). *Information Sciences, 385–386*, 225–249. https://doi.org/10.1016/j.ins.2017.01.018.

Zhang, J., Litvinova, M., Liang, Y., Wang, Y., Wang, W., Zhao, S., et al. (2020). Changes in contact patterns shape the dynamics of the COVID-19 outbreak in China. *Science, 368*(6498), 1481–1486 (New York, N.Y.). https://doi.org/10.1126/science.abb8001.